Student thesis series INES nr 390

Methane flux measurements with low-cost solid state sensors in Kobbefjord, West Greenland

Hanna Axén

2016
Department of
Physical Geography and Ecosystem Science
Lund University
Sölvegatan 12
S-223 62 Lund
Sweden

Hanna Axén (2016).
Methane flux measurements with low-cost solid state sensors in Kobbefjord, West Greenland
Mätningar av metanutsläpp med halvledarsensorer i Kobbefjord, Väst-Grönland.
Master degree thesis, 30 credits in *Physical Geography*
Department of Physical Geography and Ecosystem Science, Lund University

Level: Master of Science (MSc)

Course duration: *November* 2015 until *June* 2016

Disclaimer

Methane flux measurements with low-cost solid state sensors in Kobbefjord, West Greenland

---

Hanna Axén

Master thesis, 30 credits, in
Atmospheric Sciences and Biogeochemical Cycles

Supervisors:
Mikhail Mastepanov
Department of Physical Geography and Ecosystem Analysis,
Lund University

Torben R. Christensen
Department of Physical Geography and Ecosystem Analysis,
Lund University

Exam committee:
Jutta Holst,
Department of Physical Geography and Ecosystem Analysis,
Lund University

Daan Blok,
Department of Physical Geography and Ecosystem Analysis,
Lund University

Abstract

Methane is one of the most important greenhouse gases, and the Arctic region plays an important role in its dynamics. Due to limited observations in this remote and often harsh environments, large uncertainties surround the role of the Arctic region in a warming climate.

In this thesis, I examine the performance of the three low-cost solid state sensors, Figaro sensors TGS2600-B00, TGS2611-C00 and TGS2611-E00. These sensors could present a significant contribution in developing and expanding methane monitoring networks in the Arctic region, and furthermore improve the understanding of underlying processes controlling methane emissions. The sensors were added to the existing automatic chamber setup in Kobbefjord, close to Nuuk, West Greenland. Methane fluxes were calculated based on the change in methane concentration when chambers were closed. A reliable fast methane analyzer (RMT-200, Los Gatos Research Inc., USA) served as a proxy for methane fluxes, and the sensors' data was compared to this.

The resolution from the three sensors was limited by an analog-to-digital converter, which is expected to contribute to the larger spread in the sensors' data compared to the LGR. Occasional changes of relative humidity inside the chambers, resulted in overestimated fluxes. The experimental setup caused low relative humidity inside the syringe containing the senors. Low relative humidity is known to be problematic, which could be why no clear relationships between the sensors' signal and relative humidity and temperature were found. By filtering data with a relative humidity change $\geq$27%, most of the overestimated fluxes are most likely removed. The sensors were able to capture the seasonal trend in the methane fluxes, and the magnitude of the seasonal mean fluxes from different chambers. The results could not be statistically supported due to seasonal trends in the data and the lack of replicas.

The sensors differ in sensitivity to other deoxidizing gases. At this site, no indications of such gases were found, but this could be a problem at other sites, meaning that one of the more methane specific sensors may be suitable. Although, the TGS2600-B00 sensor showed better results in this study, further tests are required to determine which of the sensors is the best.

In conclusion, the results indicate that, these sensors with further refinements may well be used for expanding monitoring networks of methane fluxes in the Arctic.

Sammanfattning

Metan är en av de viktigaste växthusgaserna, och Arktis står för en betydande del av de naturliga metanutsläppen. På grund av få observationer och mätningar från denna region, kännetecknas dess roll i ett framtida, varmare klimat av stor osäkerhet.

I detta mastersarbete undersöker jag tre mätinstrument, halvledarsensorerna Figaro TGS2600-B00, TGS2611-C00 och TGS2611-E00, vilka har en betydligt lägre kostnad än de instrument som vanligtvis används i denna sorts studier. Detta innebär att dessa sensorer skulle kunna användas för att utvidga observationsnätverk över Arktis. På så sätt skulle förståelsen för de bakomliggande processerna och variationen i utsläpp öka. Sensorerna installerades i Kobbefjord, västra Grönland, som en del av det system med automatiska kamrar som redan fanns på plats. Metanutsläpp beräknas utifrån den koncentrationsförändring som sker då en kammare stängs. Sensorernas mätresultat jämfördes med ett pålitligt referensinstrument (RMT-200, Los Gatos Research Inc., USA) för validering.

I detta experiment begränsades upplösningen av en analog-till-digital omvandlare, och inte sensorerna själva. Detta bidrog troligtvis också till den betydligt högre spridningen i sensorernas data, jämfört med referesinstrumentet. Det visade sig att kamrarna då och då gjorde att den relativa luftfuktigheten ökade under en mätning. Då sensorerna är känsliga mot temperatur och luftfuktighet, gjorde detta att dessa mätningar gav för höga värden. Inne i behållaren, där sensorerna satt, var den relativa luftfuktigheten betydligt lägre än ute i atmosfären. Låg relativ luftfuktighet har visat sig vara problematiskt för dessa sensorer, vilket kan förklara svårigheterna med att finna och beskriva temperatur- och luftfuktighetsberoendet. Istället filtrerades data med förändring i luftfuktighet högre än 27%. Genom detta identifierades de flesta överskattade värdena.

Sensorerna följde referensinstrumentets trend genom säsongen, om än med mer spridning, och kunde påvisa skillnaden i medelutsläpp från de olika kamrarna. Dessa resultat kunde dock inte stödjas statistiskt, på grund av för få kopior och säsongstrenden i datan.

De tre sensorerna skiljer i sensitivitet till andra deoxiderande gaser. Sådana gaser tycktes inte vara närvarande i Kobbefjord, men kan visa sig vara betydande vid andra platser. Det är därför svårt att peka ut vilken sensor som borde användas i framtiden, även om TGS2600-B00 visade de bästa resultaten i denna studie. Istället skulle mer forskning kunna ge en klarare bild av när de olika sensorerna fungerar som bäst.

Sammanfattningsvis så tyder detta projekt på att dessa halvledarsensorer, efter ytterligare tester, mycket väl skulle kunna användas för att expandera och utveckla ett observationsnätverk för metanutsläpp från Arktis.

Contents

1 Introduction

The Arctic region plays an important role in global carbon dioxide (CO_2) and methane (CH_4) dynamics. It is considered to be a net source of CH_4 to the atmosphere, as a result of the wetlands, shallow lakes and saturated sediments present throughout the region (McGuire et al., 2009). Despite its relatively low atmospheric concentration, CH_4 is one of the most important greenhouse gases, due to a high global warming potential (GWP) (Stocker et al., 2013). The observational record shows how high latitudes experience an enhanced warming compared to the rest of the globe, a trend which climate models project to continue under future warming scenarios (Christensen et al., 2013). It is therefore important to understand how Arctic processes and feedbacks will respond in a warmer world. The remoteness and often harsh climate in the Arctic region limits the observations on both temporal and spatial scales. Consequently, great uncertainties surround the Arctic change and resulting CH_4 emission (Schuur et al., 2015; Christensen, 2014). By expanding monitoring networks of greenhouse gases, such as CH_4, the understanding regarding the role of the Arctic region in a changing climate could improve.

Here, I present a study examining low-cost solid state sensors, measuring CH_4, which could present a significant contribution when expanding the monitoring networks in the Arctic.

1.1 Purpose and Study Aim

The aim of this thesis is to examine whether the Figaro TGS2600-B00, TGS2611-C00 and TGS2611-E00 sensors can be used to obtain CH_4 fluxes using the automatic chamber technique. Further, I want to find out under which conditions they perform well, whether any corrections are needed and which sensor is most reliable.

The study is based on the following hypothesis:
H: *The Figaro sensors can distinguish patterns in methane fluxes, using the automatic chamber technique.*

To test the hypothesis the following study questions are set up:

- *Can the Figaro sensors resolve the seasonal pattern in CH_4 fluxes and any potential difference between chambers?*
- *Under which conditions do the sensors produce reliable results?*
- *Which sensor performs the best?*

At the Greenland Ecosystem Monitoring research site in Kobbefjord, CH_4 fluxes have been monitored since 2008 (Tamstorf et al., 2008). Its proximity to Nuuk makes it relatively accessible compared to other Arctic sites. This makes it a good location to test the sensors by adding them to the existing setup. The objective is to compare the concentrations and calculated fluxes from the Figaro sensors to a reliable instrument. Regression analysis between the sensor and the reliable instrument are done to assess the performance of the sensors. The times during which the sensors do not perform well are identified and corresponding atmospheric and soil conditions are analyzed. Correcting the data for temperature and relative humidity sensitivities are attempted. The Kobbefjord

CH_4 seasonal fluxes will only be briefly discussed in this thesis, as thorough analysis of their controls and variability are outside the scope of this project.

2 Background

2.1 Climate Change and the Arctic

The global warming observed since pre-industrial time is most likely of anthropogenic origin (Stocker et al., 2013). Globally, the Arctic region stands out with the most pronounced warming, an effect often referred to as the Arctic amplification (Serreze and Francis, 2006). This is a combined effect of several factors, such as increased moisture in the atmosphere and diminishing snow and ice cover. Increasing atmospheric moisture cause more heat transfer from low latitudes to the Arctic. Reduction in snow and ice cover increase the heat absorption by open ocean, which cause further melting, known as the ice-albedo feedback (McGuire et al., 2006). The projections by global climate models point towards a continuation of this enhanced Arctic warming trend, with temperature increases of several degrees by the end of this century (Serreze and Francis, 2006; Christensen et al., 2013; Vaughan et al., 2013).

The Arctic cryosphere has undergone drastic changes over the last decade. The decrease in sea ice extent has been faster than most global climate models have predicted (Erich et al., 2013). Loss of sea ice could have various implications, such as on the Arctic carbon cycle, as CH_4 emissions can be affected by warming caused by the ice-albedo feedback (Parmentier et al., 2013). Glaciers are shrinking globally, and snow cover is decreasing in both extent and duration (Vaughan et al., 2013; Saito et al., 2013). Over the Arctic, an overall increase in precipitation, particularly in winter, is projected (Christensen et al., 2013). This Arctic warming has already affected physical and ecological systems in this region, some of which may be irreversible on century time scales (McGuire et al., 2009).

2.2 Permafrost and carbon

Permafrost is defined as ground frozen for more than two consecutive years, and underlies much of the Arctic region. Overlying the permafrost, is the active layer which thaws every year. The thickness of permafrost and the overlying active layer can vary greatly, where the thickest permafrost can be around 1 km and active layers can vary in depth from a few centimeters to several meters (Hanne Christensen, pers. comm. 2012). Observational records of permafrost temperatures reveal a warming trend since the 1980s (Vaughan et al., 2013). Particularly minimum temperatures of cold permafrost have increased. The higher temperatures combined with changes in snow cover and duration has resulted in permafrost degradation around the Arctic (Saito et al., 2013). The snow plays an important role in permafrost dynamics, by acting as an insulating layer, both against warmth and cold. When the snow duration decreases, permafrost is exposed to warm temperatures during a longer period, which enhances thaw. Precipitation increase during the winter season, as projected by global climate models, could cause the snow cover to thicken and consequently insulate from cold temperatures. As a result minimum temperatures of the permafrost rise. Experimental increases of snow depth resulted in soil temperature increase, active layer thickening and surface subsidence (Johansson et al., 2013).

Permafrost can degrade in various ways (Schuur et al., 2008). Higher temperatures penetrate deeper into the ground, thaw the permafrost from above, and thus increase the active layer thickness. Development of taliks, unfrozen ground surrounded by continuous permafrost, can take place when the active layer has become deep enough to inhibit

complete freezing during winter. Abrupt changes can be seen when ice rich soils thaw and collapse, resulting in so called thermokarst formation. This alters the soil hydrology locally and can produce shallow lakes or enlarging already existing ones. Warming may cause the thawing soil to detach from underlying bed and erode or slip (Vaughan et al., 2013).

Large quantities of carbon, accumulated over thousands of years, are stored in the Arctic. Permafrost regions are estimated to contain twice as much carbon as currently stored in the atmosphere (Schuur et al., 2015). Despite only accounting for 15% of the terrestrial land surface, these regions could represent 1/3 of the global soil carbon pool. Large uncertainties surround the estimations of Arctic carbon storage (McGuire et al., 2009).

As permafrost thaws, previously trapped carbon becomes available for microbial decomposition, enhancing carbon emissions. The permafrost-carbon feedback refers to this positive loop of warmer temperatures leading to enhanced emission of greenhouse gases which further increase warming. This represents one of the most important feedbacks between terrestrial ecosystems and the climate (Schuur et al., 2008). The future size and impact of the permafrost-carbon feedback will depend on how the anthropogenic emissions change; 2/3 of the emissions could be avoided by following the lower emission scenario (RCP4.5) compared to the highest (RCP8.5) (McGuire et al., 2006). As a consequence of the Arctic amplification, the Arctic is the region with the largest temperature difference between the emission scenarios (Stocker et al., 2013). The Arctic is currently acting as a net carbon sink (McGuire et al., 2009), but there are indications of a gradual transition into a carbon source (Erich et al., 2013; Schuur et al., 2015). Once the permafrost-carbon feedback is going, it could be irreversible on a millennial scale (Erich et al., 2013). Abrupt changes and catastrophic emission events are unlikely to occur (Parmentier and Christensen, 2013). According to Schuur et al. (2015) 5-15% of the terrestrial permafrost pool could be released by the end of this century, dominated by CO_2 release although the warming potential increases by accounting for CH_4 emissions. Estimated to account for 2.3% of the carbon release from permafrost soils by 2100, CH_4 would account for 1/3 to 1/2 of the climate forcing of these emissions (Schuur et al., 2013).

The high GWP makes CH_4 one of the most important greenhouse gases, after CO_2 and H_2O, despite its relatively low atmospheric concentration (Stocker et al., 2013). Its GWP describes how much energy a molecule of CH_4 adds to the Earth's energy balance, compared to a molecule of CO_2. CH_4 has a relatively short atmospheric lifetime, around 12.4 years, which makes the GWP differ depending on time horizon, but also whether the carbon cycle feedback is included or not. The GWP for CH_4 ranges between 28 and 84 (Myhre et al., 2013).

High quality, easily decomposable carbon that becomes available with permafrost thaw may have an enhancing effect on the emissions over the course of a few years up to a decade - an effect which would diminish without further thaw and exposure of new carbon (Schuur et al., 2015). Uncertainty remains regarding the rate at which it will become available for decomposition, and its decomposability (McGuire et al., 2009). The permafrost-carbon feedback can have implications for the global climate, although its impact is overshadowed by fossil fuel emissions (Schuur et al., 2013).

2.3 Methane related processes

The atmospheric CH_4 concentrations have increased by about 150% since pre-industrial levels. This is attributed mostly to anthropogenic emissions from biomass burning, agriculture, waste and fossil fuels (Myhre et al., 2013). The natural CH_4 sources are dominated by wetlands (Ciais et al., 2013). The Arctic represents an important CH_4 source due to its significant cover of wetlands and shallow lake systems (McGuire et al., 2009).

Carbon decomposed in aerobic soils is released as CO_2, whereas anaerobic environments enable CH_4 production and release. Microbial decomposition of carbon is affected by substrate availability and decomposability, as well as various environmental factors such as soil temperature, soil moisture, available nutrients and oxygen levels (Schuur et al., 2008, 2015; Ström et al., 2015). The future of the Arctic carbon cycle is dependent on how the hydrological conditions change, in association to e.g. permafrost thaw, as previously discussed (Schuur et al., 2015).

Wetlands, lakes and waterlogged soils provide anaerobic conditions in which CH_4 production is possible. Methanogenic bacteria, methanogens, thrive in the absence of oxygen and CH_4 is produced through their metabolism. For methanogens to be metabolically active, temperatures above 4-5℃ are required (Blake et al., 2015), but the optimum temperatures for methanogenesis are as high as 30℃, which is significantly higher than what can be expected in Arctic environments. The production often takes place in deeper sediments from which it can be transported in various ways to the atmosphere. Release rates of CH_4 are often one to two orders magnitude lower than CO_2 emission rates (Schuur et al., 2008). This is related to the transport routes via which CH_4 escapes to the atmosphere, along which oxidation into CO_2 could occur. Molecular diffusion presents a route which is rather slow, and often related to a high chance of oxidation along the way. Ebullition, the release of CH_4 as bubbles, can be an important mechanism at some sites. Plant-mediated transport is often considered the most important way of transport, and an important control of CH_4 emissions (Ström et al., 2012; Mastepanov et al., 2013). Vascular plants present an escape route from the deeper sediments to the atmosphere, which enable more CH_4 to be released without oxidation. Other factors controlling CH_4 emission are soil temperature, water table depth and substrate availability, of which the relative importance seem to vary between sites and temporally (Christensen et al., 2012; Mastepanov et al., 2013; Ström et al., 2015).

2.4 Observed and modeled CH_4 emissions

CH_4 fluxes can be measured and estimated in different ways. Chamber methods work on small scales and can improve understanding of controlling factors and underlying processes. Eddy covariance towers provide information about the gas exchange over larger scale, of size depending on the tower height (McGuire et al., 2009; Tagesson et al., 2013) but also environmental conditions, such as atmospheric stability, wind speed and vegetation.

Arctic wetlands typically represent net carbon sinks, but are net CH_4 sources (Bäckstrand et al., 2010; Christensen et al., 2012). Seasonal patterns in CH_4 emissions can vary greatly between sites but also interannually at the same site. In Zackenberg, northeast Greenland, multi-year records display substantial interannual variability during the first part of the growing season, while the later part of the season often followed a similar pattern (Mastepanov et al., 2013).

Large CH_4 emissions have been observed associated with freeze-in at permafrost sites. The bursts were on some years of similar magnitude as the cumulative emissions throughout the growing season (Mastepanov et al., 2013). The conditions required for these bursts to occur have been discussed, as they do not occur every year and vary in magnitude. The ventialting effect by vascular plants could reduce stored CH_4 in the soil and the size of succeding burst would thus be reduced (Christensen et al., 2012). Pirk et al. (2015b) found that these bursts are the effect of gas reservoirs being compressed when freezing occurs and later cracking of the soil. With this explanation, no autumn bursts are expected from permafrost free soils.

Jackowicz-Korczyński et al. (2010) conducted full-year CH_4 eddy covariance measurements on an subarctic mire in northern Sweden and found that 65% the CH_4 fluxes occurred during the growing season, 25% came from shoulder seasons and 10% was emitted during winter. This highlights the importance of conducting year round measurements of CH_4 fluxes, as release is not uniformly distributed. So called methane hotspots have been identified which can be sporadically active (Christensen, 2014). Active spots can be related to thermokarst collapses forming wetlands or lakes, but also degrading shallow subsea permafrost can emit CH_4 bubbles in a sporadic manner (Schuur et al., 2015; Shakhova et al., 2013). The lacking knowledge behind the variability in space and time contributes to the uncertainty regarding the potential impact from the Arctic region on the global climate. This accentuates the importance of further research and quantification of such hotspots and their behavior.

Modeling can present a tool to assess the response of ecosystems in under future climate scenarios. Over the last years, process-based models are increasingly incorporating the complex effects that permafrost has CH_4 processes and the carbon cycle (Hayes et al., 2014; Tang et al., 2015). Although, gaps in understanding of underlying processes still limit and brings uncertainty into the models, something which could be improved by more observations. Uncertainty in the processes governing CH_4 release are partly due to the remoteness and thus scarcity of data (Schuur et al., 2015). Due to the long response time of the system almost 60% of the emissions can be expected to occur after 2100 (Schuur et al., 2015). It is therefore important to have long-term monitoring projects. Development of long-term, year-round, ground based observational records for a multitude of various representative sites throughout the Arctic would provide data to improve the understanding of processes governing CH_4 production, and the temporal and spatial variability of CH_4 emissions (Christensen, 2014; Mastepanov et al., 2013; McGuire et al., 2009).

By examining alternative instruments, setups and techniques, development and enlarging of observational networks in the Arctic region is most likely possible. I consider the three Figaro sensors examined in this project to be such potential candidates. Therefore, this project focus on the technical assessment of these sensors; to understand if they can be used to measure methane fluxes throughout the Arctic.

3 Materials and Method

3.1 Study site

The field work was conducted at the head of Kobbefjord (64°8', 51°22') in West Greenland, close to the capital Nuuk. The site has a typical low-arctic climate with mean annual temperature of -1.4℃ and mean annual precipitation of 752 mm (1961-1990)(Thorsøe et al., 2008). Mountains up to 1400 m.a.s.l confine the 32 km^2 drainage basin. The study was conducted at a fen at where no permafrost is present. The fen vegetation is dominated by *Carex rariflora, Scirpus caespitosus, Eriophorum angustifolium* and *Vaccinium uliginosum* (Bay et al., 2008).

3.2 Figaro Sensors

Three different Tagushi Gas Sensors (TGS, Figaro Engineering Inc., Osaka, Japan) were evaluated in this project. These low-cost solid-state sensors TGS2600-B00, TGS2611-C00 and TGS2611-E00 are later referred to as Sensor 1, 2, and 3, respectively. These sensors cost around 10-15 USD, which is orders of magnitude less than other instruments commonly used for this kind of measurements. Their low power requirements and small size adds further advantages.

The three sensors should be equally sensitive to CH_4, but differ in their sensitivity to other compounds, although, as discussed later, each sensor has its own individual characteristics, which mean that the sensitivity can vary slightly between different sensors. TGS2600-B00, sensor 1, was developed as a smoke detector sensitive to various air contaminants, such as hydrogen and CO, but also CH_4 and ethanol. The two TGS2611 sensors (sensor 2 and 3), are primarily sensitive to CH_4 and have reduced sensitivity to other gases. The TGS2611-E00, sensor 3, has a filter that should lower the sensitivity to ethanol and iso-butane even further. Typical sensitivity to various gaseous compounds can be seen in Figure 1. A linear relationship was assumed for the scope of this project, in line with previous studies (Eugster and Kling, 2012).

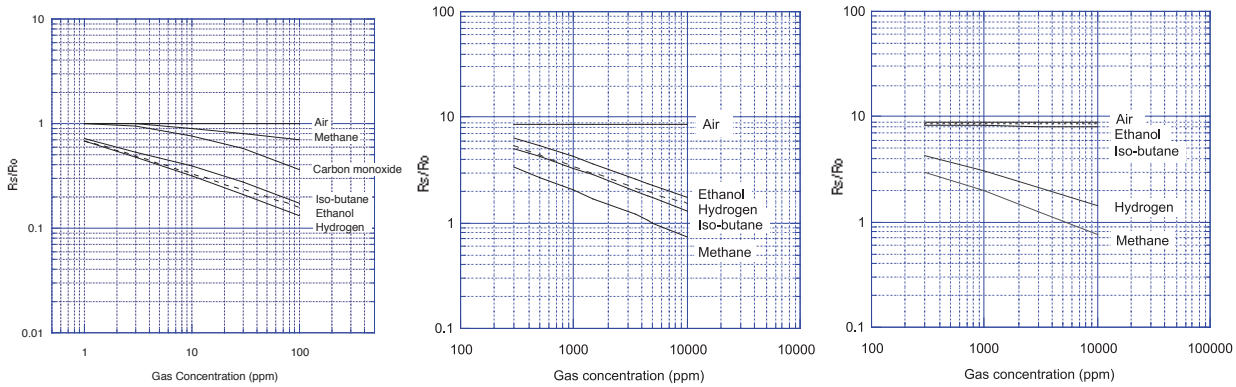

(a) Sensor 1, TGS2600 **(b)** Sensor 2, TGS2611-C00 **(c)** Sensor 3, TGS2611-E00

Figure 1: Sensitivity characteristics for the three Figaro sensors. The plots describe the resistance depending on concentration of different gases. Note the difference in scale for Sensor 1. The characteristics represent typical values at 20℃ air temperature and 60% relative humidity (Figaro USA Inc., 2005b, 2013). Expected CH_4 range in this project is between 1 and 5 ppm, which outside the typical detection range for Sensor 2 and 3 presented by Figaro USA Inc. (2013).

The Figaro sensors are thick film metal oxide semiconductors, commonly used as air quality control sensors. The basic structure of the three sensors is the same. A metal oxide crystal (SnO_2) is used for sensing material. The sensors have a heater to keep the temperature stable at a level where oxygen adsorbs onto the crystal surface. Oxygen is strongly electronegative and attracts the crystal's electrons, which increases the resistance. In the presence of a deoxidizing gas, some oxygen will be removed from the crystal surface, which lowers the resistance. The reduced resistance can be related to the concentration of the deoxidizing gas.

Each sensor has an individual resistance in clean air, R_0. The resistance drop in the presence a deoxidizing gas is described by equation (1) (Figaro USA Inc., 2005a).

$$R_s = A \cdot [C]^{-\alpha} \tag{1}$$

where R_s is the resistance of the sensor, A is a constant, $[C]$ is the concentration of the de-oxidizing gas and α is the slope of the resistance-concentration curve (Figure 1). To determine R_s an electric circuit was setup according to Figure 2. A load resistor (R_L) was connected in series to the sensor. A change in sensor resistor indirectly affects the voltage (V_{RL}) over the load resistor. V_{RL} was measured and can be used to obtain R_s (equation (2)).

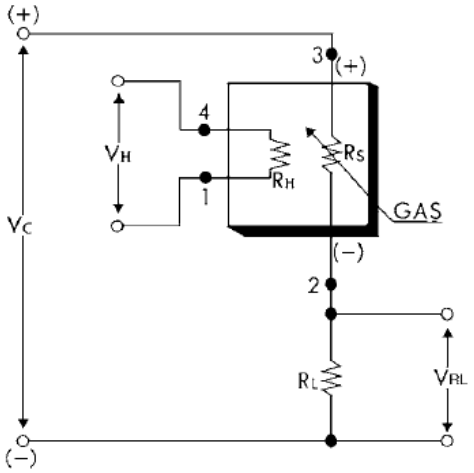

Figure 2: Basic measuring circuit setup for the Figaro sensors (Figaro USA Inc., 2012b).

$$R_s = \frac{V_c \times R_L}{V_{RL}} - R_L \tag{2}$$

where V_c is the supple voltage of 5V, R_L is precision resistor of 5Ω and V_{RL} is the measured voltage. Reduction in resistance results in a corresponding increase in measured output voltage. By rearranging equation (2), inserting R_s from equation (1) and assuming $\alpha = 1$ (Eugster and Kling, 2012; Figaro USA Inc., 2005a), equation (3) is obtained where the output voltage linearly dependent to the concentration.

$$V_c = V_{RL}\left(\frac{A \cdot [C]}{R_L} + 1\right) \tag{3}$$

Temperature influences the chemical reaction rate of which gases are adsorbed or desorbed from the crystal surface. Higher temperature yields lower resistance. Molecules of water

vapor get adsorbed onto the surface which decreases the resistance, which means that the sensors are sensitive to changes in humidity. Each sensor has its individual characteristics which means that coefficients, used to correct for relative humidity and temperature, and to convert to desirable units, had to be calculated for each sensor(Figaro USA Inc., 2005a).

TGS2600 sensors were tested by Eugster and Kling (2012) in Alaska, by comparing the sensor data to one minute averages of open air concentration data, measured by a Los Gatos Research FMA 100. With this measurement technique, changes in concentration were used to estimate fluxes from the nearby lake and surrounding areas. Temperature and relative humidity changes had large effects on their readings, and an empirical formula was developed to correct for these dependencies. They found that the general behavior of the sensors was lost with relative humidity below 35%, and therefore they excluded data below 40% relative humidity. After performing these corrections, the data from the sensor compared reasonably well to their reference instrument. The quality of the data was concluded to be sufficient for preliminary studies detecting spatial heterogeneity in CH_4 fluxes.

According to the manufacturer the resistance of the sensors drops quickly when exposed to deoxidizing gas, the response is almost immediate, while it takes some seconds for the sensors to stabilize at the new signal. The recovery of the signal is extended over a longer time period, typically less than a minute (Figaro USA Inc., 2005a). TGS2611-E00 has an overall slower response as an effect of the filter; examples presented by the manufacturer indicate almost a minute before the signal has stabilized after exposure and closer to two minutes before the signal has recovered. The sensors show a sharp drop in resistance the first seconds after the sensor is turned on after longer unenergized storage, known as initial action. The duration of the initial action depends on storage conditions and length. The signal generally stabilizes after a few minutes. When tested over a 500 day period, the TGS sensors showed stable signal (Figaro USA Inc., 2005a).

3.3 Measurement setup

Methane fluxes have been monitored in Kobbefjord since the installation of six automatic chambers in August 2007 (Tamstorf et al., 2008). Automatic chambers are used at various sites around the Arctic region for CH_4 flux measurements (Pirk et al., 2015a). The location of the chambers and instruments can be seen in Figure 3. Due to technical issues, only four of the chambers, number 1, 2, 5 and 6, operated during the 2015 season. At the site is also the INTERACT weather station and the SoilFen station, measuring soil properties and weather conditions.

The chambers consist of an aluminum carcass with Plexiglas walls, and the motor-driven lid. The base is 60 cm $\times$ 60 cm and the height 30 cm. The lid opens and closes automatically according to the schedule specified in Table 1. Each chamber operates once every hour. The chambers stay open when inactive. A fan, attached to the wall inside each the chamber, makes sure that the air gets properly mixed. The fan mixes the air during the full 10 min period of its active chamber. Air is pumped from the active chamber via polyethylene tubes to the instruments and then back to the chamber, at a flow rate of 0.4 L min^{-1}, (Mastepanov, 2009; Pirk et al., 2015a). Tubes were attached to the non-working chambers to pump ambient air rather than air from the wooden box to the instruments. All tubes and cables go through hardy rubber-covered hoses to protect against foxes.

The CH4 concentration is measured at a frequeency of 1 Hz, by a non-destructive

fast methane analyzer (RMT-200, Los Gatos Research Inc., USA), which is later referred to as LGR. The LGR is used at several sites of this setup (Pirk et al., 2015a), and is considered to provide reliable CH_4 concentration measurements. An IBM computer with OS Linux Red Hat, referred to as LGR computer, operates the LGR, valves, motors and some other instruments. An analog-to-digital converter, LabJack U3, connects devices to the LGR computer. All the instruments are installed inside a Zarges box, placed in the wooden box for protection against weather. To prevent overheating, the lid of the Zarges box was kept slightly open by a wooden stick.

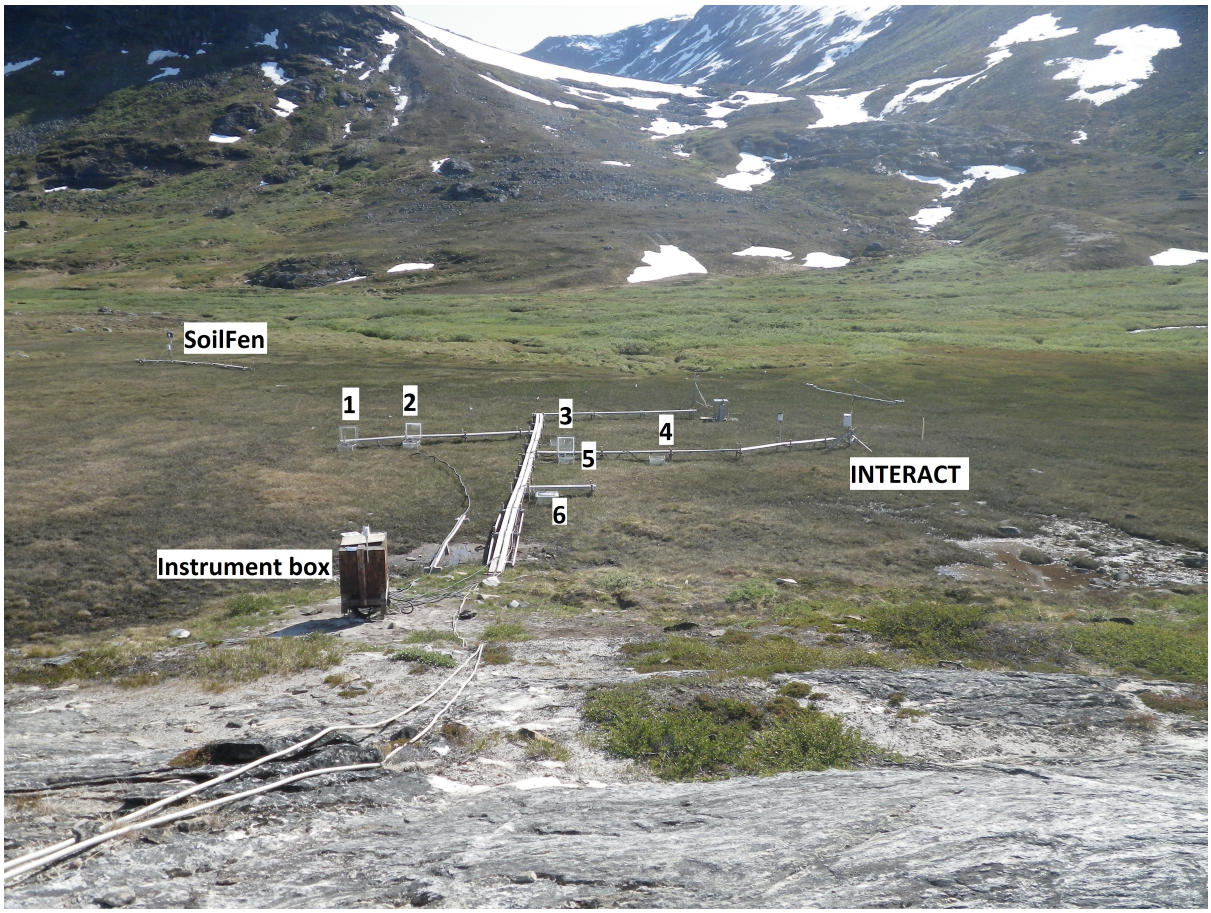

Figure 3: Photo of the fen site in early July, 2015. The numbering of the chambers and the instrument box is marked as well as the SoilFen and INTERACT stations. The tubes transport the air from the chambers to the instruments inside the wooden box. Photo taken by the author.

Table 1: Work schedule of the chamber, adopted from Mastepanov (2009), describing when the each chamber is active, and when the lids open and close.

Time (hh:mm)	Active chamber	State
*:00 - *:10	1	
*:00 - *:03		Chamber open
*:03 - *:08		Chamber closed, used for flux calculation
*:08 - *:10		Chamber open
*:10 - *:20	2	The same schedule:
*:20 - *:30	3 (not operating 2015)	*:*3 – chamber closes,
*:30 - *:40	4 (not operating 2015)	*:*8 – chamber opens
*:40 - *:50	5	
*:50 - *:00	6	

For the purpose of this study, the three Figaro sensors were added to the existing setup. Sensors measuring pressure STD-015-A (Sencera Co. Ltd, Taipei, Taiwan), air temperature SMTIR9902 (Smartec BV, Breda, The Netherlands) and relative humidity HIH-4000-003 (Honeywell International Inc., Minneapolis, USA) were placed in a syringe together with the Figaro sensors (Figure 4). Air tubes were attached on each side of the syringe for air to pass through before reaching the LGR. The syringe was placed in a foam padded cardboard box to keep temperature stable.

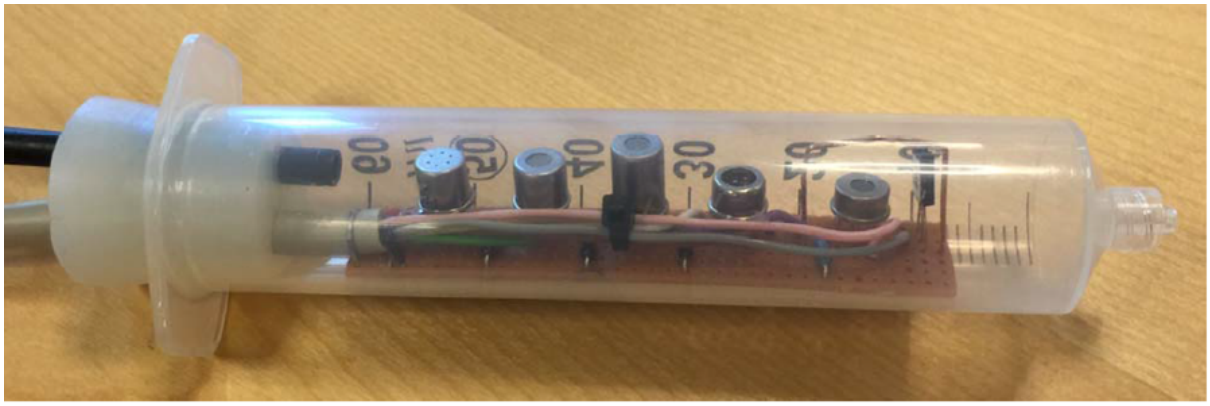

Figure 4: The syringe containing the sensors, from left to right, TGS2600-B00, TGS2611-C00, TGS2611-E00, temperature, relative humidity and pressure. Photo taken by Mikhail Mastepanov.

3.4 Data Analysis

3.4.1 Collected Data

The CH_4 concentration was measured by the LGR and the Figaro sensors at a frequency of 1 Hz. The LGR concentration is given in [ppm], and the output signal from the Figaro sensors in [mV]. This output voltage is used as a proxy for CH_4 concentration throughout most of the analysis, until conversion coefficients were obtained.

Data from the Greenland Ecosystem Monitoring Programme were provided by the Department of Bioscience, Aarhus University, Denmark in collaboration with Department of Geosciences and Natural Resource Management, Copenhagen University, Denmark (obtained from GEMdatabase (2016)). Description of the analyzed data, from the SoilFen and INTERACT stations, follows:

- SoilFen recorded at a frequency of 1 measurement every 5 minutes until the 15th of July at 09:30 AM, after 10:28 AM of that day, the frequency was increased to 1 per minute. Proving air temperature, relative humidity, soil temperature, photosynthetic active radiation (400-700 nm, PAR)
- INTERACT recorded once every 30 minutes. Providing air temperature, soil temperature, pressure, rain, soil moisture, net radiation

3.4.2 Flux calculation

Methane fluxes were estimated from the concentration change during the time when the chambers were closed. The calculations were done using DataShow for Windows (author: M. Mastepanov) assuming constant emission rates, seen as a linear concentration change. The validity of this assumption has been discussed (Juszczak, 2013). Assessments of its validity against other models concluded the linear model to be appropriate for this purpose (Pirk et al., 2015a). DataShow performs a linear regression on the concentration data from the LGR. It automatically identifies and uses the most linear part of the concentration curve for each 10 minute slot. The flux is the slope of this section. The regression time interval was changed manually if unrepresentative, or marked as 'bad' if a flux had to be disregarded, e.g. due to missing data or unstable signal, indicating improper seal of the chamber lid. Erroneous measurements, 'bad'-marked or '9999'-values, were excluded from further analysis. Also sensor fluxes of '0' were excluded, due to their problematic effect on some calculations. Ebullition was not considered in this analysis, and sudden rises in concentration from potential bubble events disregarded.

Fluxes were calculated for the Figaro sensors for the same time interval. Since the program automatically chose the time interval only considering the LGR, the data had to be carefully reviewed and the time interval changed when it did not match the sensors' concentration curve. Due to the influence of relative humidity on the sensor signal, the time interval also considered the time of most stable relative humidity. To reduce subjectivity the automatic choice was preferred and kept whenever possible. If the signal from the Figaro sensors did not show a linear response the automatic time slot was used.

The data from the sensors was analyzed as output voltages [mV], and not converted to R_s/R_0 as described by Eugster and Kling (2012).

3.4.3 Analysis of Figaro sensors performance

Data handling and analysis was done in MATLAB version 8.5.0.197613 R2015a (The MathWorks, Inc., Natick, MA, USA) and RStudio (R Core Team, 2015). The LGR was used as a proxy for CH_4 concentration change, and served as comparison for validation of the Figaro sensors throughout the analysis.

For comparison of the data spread the standard deviation of the standardized residuals was calculated according to equation (4).

$$std_{res,i} = std\left(\frac{F_i}{\mu_{F_i}} - \frac{LGR}{\mu_{LGR}}\right) \tag{4}$$

where F_i is the Figaro sensor flux, μ_{F_i} is the mean of F_i, i represents Figaro sensor 1, 2 or 3, LGR is the LGR flux and μ_{LGR} is the mean LGR flux. This accounts for the different magnitudes of the sensor outputs.

Outliers were identified when being further from the linear regression line than a specified threshold. To obtain thresholds for each sensor depending on their relative magnitude, an approach according to equation (5) was performed. This outlier data was used to analyze the conditions producing unreliable readings from the Figaro Sensors (Section 3.4.5).

$$Outlier_{limit,i} = 2 \cdot std_{res,i} \cdot \mu_F \tag{5}$$

The sensor data was also filtered based on the change in relative humidity ($\Delta RH = RH_{max} - RH_{min}$) inside the syringe. Three different time frames were tested with various thresholds to find the best way of identifying outliers:

- ΔRH1: the 10 minutes period
- ΔRH2: the 5 minutes when the chamber is closed
- ΔRH3: the interval used for the flux linear regression

Finally, ΔRH3 was used with a threshold value of 50 mV, which corresponds to a relative humidity change of 27%. Hereafter, this filtering method is referred to as ΔRH-filtering. Daily mean fluxes from the ΔRH-filtered data were calculated for the period 15th of July to 30th of September.

To sum up, the following datasets were obtained:

- Raw, unfiltered data
- *Outlier*-filtered data
- ΔRH-filtered data
- ΔRH-filtered daily means (15th July - 30th of September)

3.4.4 Regression Analysis

Scatter plots of LGR versus Figaro sensor fluxes were produced. First order polynomial regressions were made for each Figaro sensor dependent on the LGR. Three data sets were tested: (1) the raw fluxes, (2) the ΔRH-filtered fluxes and (3) the ΔRH-filtered daily fluxes. Thereafter, the ΔRH-filtered datasets were examined with a polynomial regression model of second order.

The data was evaluated for the assumptions for regression, as stated below (Rogerson, 2001):

Assumption	Evaluation
1. Polynomial relationship between x and y Here as first order ($y = a_1 + a_2x$) and second order ($y = b_1 + b_2x + b_3x^2$)	Scatter plots
2. Normal distribution of the errors around the regression line, for each x-value.	Quantile-quantile plots (Q-Q plots)
3. No auto-correlation: independent residuals	Assessed with regards to the experimental setup
4. Homoscedasticity: The errors have mean of zero and a constant variation. The errors do not vary with x.	Residuals versus fitted values plot

Potential significant differences between the sensors were examined by an Analysis of Variance (ANOVA) between their regressions. ANOVA also tested if there were any significant difference between the linear and second order polynomial regressions.

The ΔRH-filter was applied and the sensor fluxes were converted by the regression coefficients obtained from the daily ΔRH-filtered data (equation (6)).

$$F_{ppm\ min^{-1}} = (F_{mV} - a_1) \cdot \frac{1}{a_2} \tag{6}$$

where $F_{ppm\ min^{-1}}$ is the flux in [ppm min^{-1}], F_{mV} the flux in [mV] and, a_1 and a_2 are the first order polynomial regression coefficients from the daily ΔRH-filtered data.
Conversion into more commonly used flux unit [mg CH_4 m^{-2} h^{-1}] was done by equation (7). This conversion accounts for temperature and pressure, according to the ideal gas law.

$$F = F_{ppm\ min^{-1}} \cdot \frac{60}{10^6} \cdot h \cdot \frac{M_{CH_4} \cdot P}{R \cdot T} \cdot 10^3 \qquad [\text{mg } CH_4 \text{ m}^{-2} \text{ h}^{-1}] \tag{7}$$

F is the flux [mg CH_4 m^{-2} h^{-1}], $F_{ppm\ min^{-1}}$ the flux [ppm min^{-1}], h the height of the chamber [m], M_{CH_4}=16 the molar mass for CH_4 [g mol^{-1}], T is the air temperature [K], P is the air pressure [Pa] and R=8.314 is the universal gas constant [Pa m^3 mol^{-1} K^{-1}].

As a final step, the seasonal mean flux by chamber was calculated for each instrument, and presented together with the ratio between the sensors' mean and standard deviation compared to the LGR.

3.4.5 Relative humidity and temperature dependence

The outliers from Sensor 1, captured by the *Outlier*-filter, were compared to the weather data from INTERACT and SoilFen stations. Temperature, relative humidity, pressure, PAR, soil moisture and radiation was analyzed for threshold values that could explain the outliers. Time series of each measure were made with the times for marked outliers, as a visual assessment.

The signal from the temperature and relative humidity sensors inside the syringe were converted from [mV] to their respective SI-units according to their calibration certificates.

Post-field laboratory tests of the sensors response to changes in relative humidity and CH_4 were made.

The resolution of the Figaro sensors was limited by the 12 bits analog-to-digital converter, which has a resolution of 4.883 mV. The resolution corresponding to each sensor, due to the analog-to-digital converter, was also calculated based on equation (6), with F_{mV}=4.883 mV.

A model in the form of equation (8) was used to correct the sensor signal for relative humidity and temperature, based on the work of (Eugster and Kling, 2012). Representative 10 minute measurements with clear increases in relative humidity were selected for this analysis. Coefficients were obtained for the measurements individually and compared with the purpose of finding the ones with the best general fit.

$$LGR = F \cdot (a + b \cdot RH + c \cdot T) + d \tag{8}$$

4 Results

Four of the six chambers functioned during the 2015 season. The data record from chamber 1 and 6 starts on the 28th of June, and chamber 2 and 5 starts on the 30th of June. Data is missing for chamber 1 between July 10 16:00 and July 14 9:40, due to stormy conditions which caused the chamber 1 lid to stay closed. The Figaro sensor record starts on the 28th of June, but is not continuous until after the 14th of July. After the 14th of July, the data set does not contain any major breaks, and the system was shut down on the 17th of October.

The seasonal CH_4 fluxes and the results of the regression analysis are presented, followed by the analysis of the relative humidity and temperature dependence.

4.1 Seasonal patterns in the CH_4 fluxes

The CH_4 fluxes from the LGR are presented in Figure 5a. Chamber 1 had the highest fluxes throughout the season, while the other chamber fluxes were of similar magnitude. The seasonal peak in CH_4 fluxes occurred around the 10th of July, after which the fluxes diminished until the end of the season. Temperatures below zero occurred between the 4th and 9th of October, resulting in freezing of the top 2 cm soil layer (Figure A15, Appendix A). A small burst of increased fluxes succeeded this period, as the temperature rose again. Fluxes displayed a diurnal pattern with higher emissions during daytime and lower during night. The fluxes from the three Figaro sensors are presented in Figure 5b-d. The y-axes are set to visualize the seasonal trend, and these plots do therefore not show all outliers. The seasonal pattern from the LGR is seen in the sensor data, although the spread is greater for the sensors.

The scatter plots in Figure 6(a)-(c) show the covariance of the unfiltered sensor fluxes compare to the LGR fluxes. The majority of data points are gathered around the linear regression line with some spread, but overestimated and a few underestimated fluxes are present in the data. The *Outlier*-filter removed 2.91% of the fluxes for Sensor 1, these removed data were used for analysis of corresponding conditions.

Figure 6(d)-(f) show the corresponding results for the ΔRH-filtered data. This filter removed 5.5% of the data, most of which were distinguished as over- or underestimations, but also a few occurrences within the acceptable range (Figure 7). The ΔRH-filtered data is spread throughout the season. Higher overestimation of fluxes were found during the first half of the season. Stable signal without outliers occurred during a period from the end of August to mid-September. This coincided with a period of frequent rain from 28th of August to 7th of September. Daytime between 4th and 12th October, these conditions occurred particularly frequently. Of the marked data approximately 2% are underestimated compared to the LGR. The number and percentage of ΔRH-filtered data from each chambers are presented (Table 2). Chamber 2 contributed the majority of all ΔRH$\geq$27 % occurrences. The first and second order polynomial regressions for the daily, ΔRH-filtered data from Sensor 1 is presented in Figure 8(a) and (b).

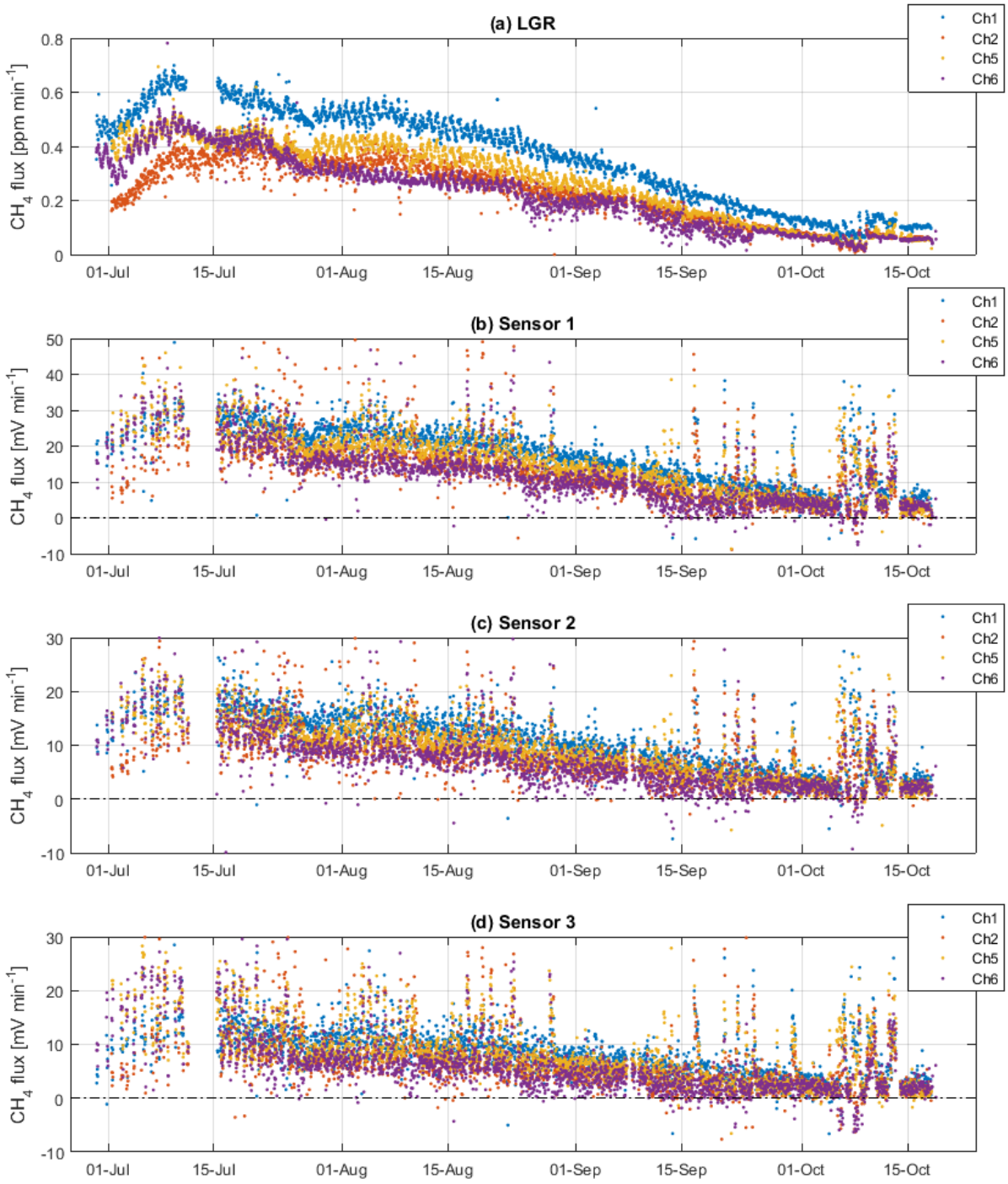

Figure 5: Methane unfiltered fluxes from the LGR [ppm min^{-1}] and the Figaro sensors [mV min^{-1}], colors represent the different chambers. The y-axes are set to focus on the seasonal pattern and all outliers from the Figaro sensors are therefore not seen. Daily patterns in the LGR fluxes show higher fluxes during daytime compared to night.

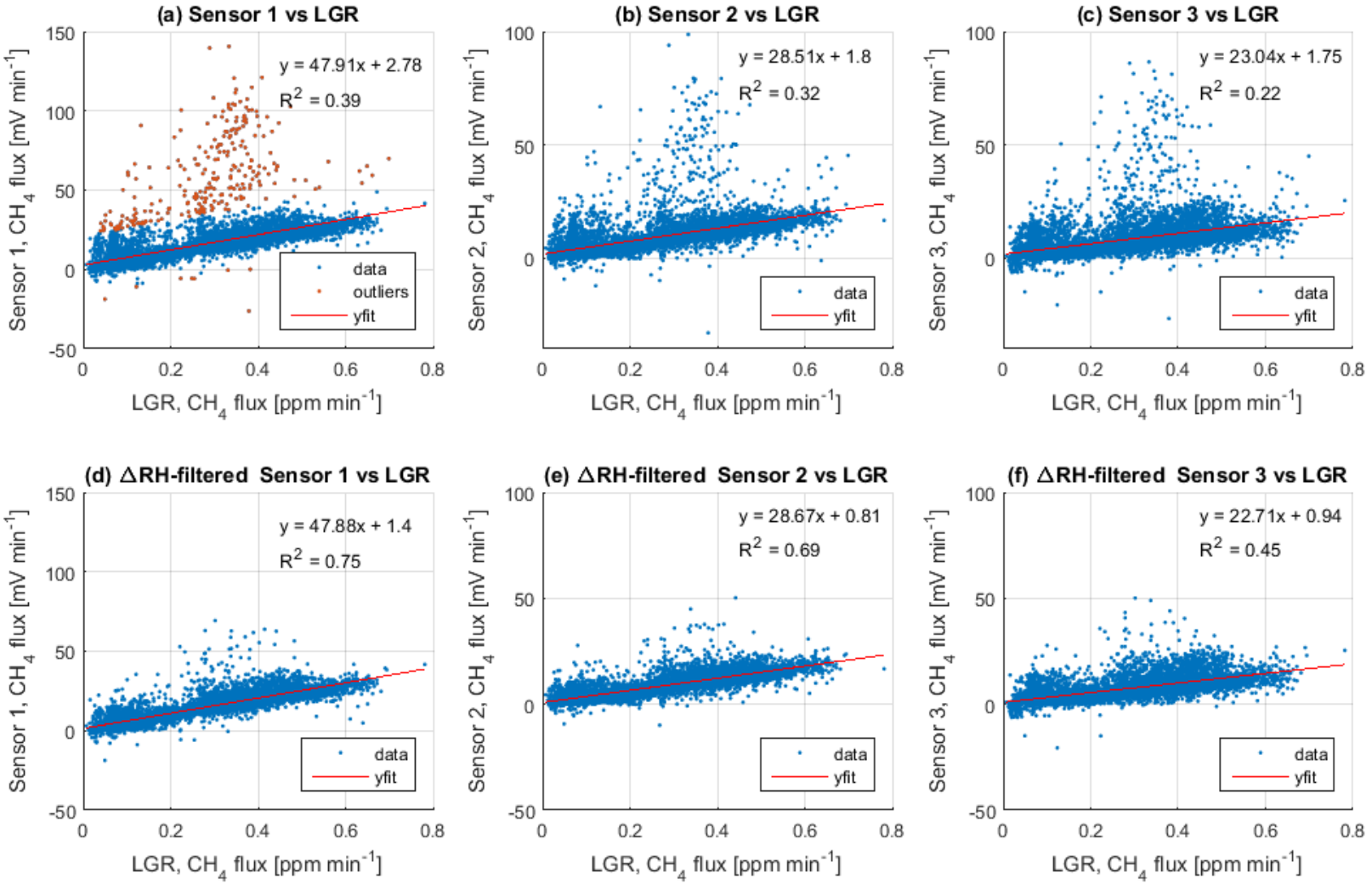

Figure 6: Scatter plots of the CH_4 fluxes from the Sensors against the LGR. The linear regression equation and corresponding R^2-value is presented in respective plot. (a)-(c) show the unfiltered data for Sensors 1-3. Data identified by the *Outlier*-filter, for analysis of conditions causing unreliable sensor data, is marked orange in the Sensor 1 plot(a). (d)-(f) show the corresponding plots for the ΔRH-filtered data. The highest R^2-value was obtained for Sensor 1 in both cases.

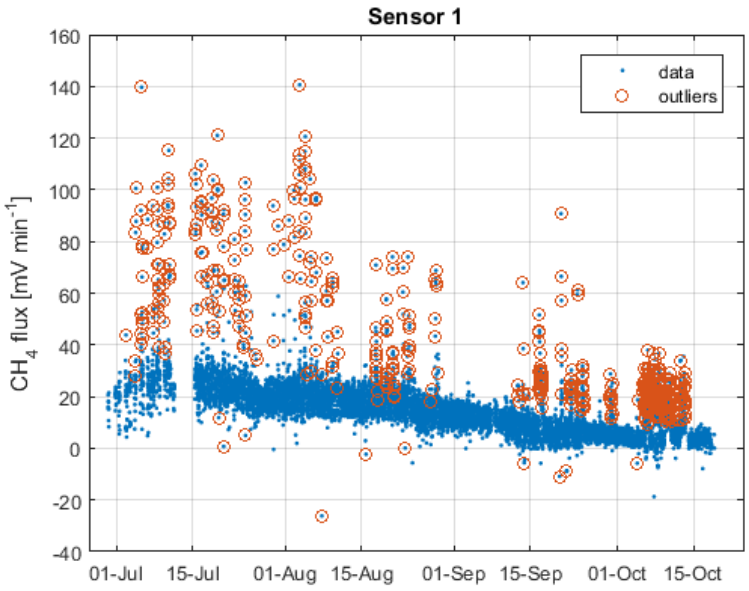

Figure 7: ΔRH-filtering of the sensor 1 data, using a threshold of 27 % relative humidity change in relative humidity for the time interval used in the flux calculation. This identified 5.5 % of the data, marked with orange circles.

Table 2: Number of measurements with RH≥27 %, thus dismissed data, from the different chambers, and their relative contribution.

	Chamber 1	Chamber 2	Chamber 3	Chamber 4
ΔRH≥27 %	29	156	34	51
% of total	10.7	57.8	12.6	18.9

Sensor 1, 1st order polynomial regression

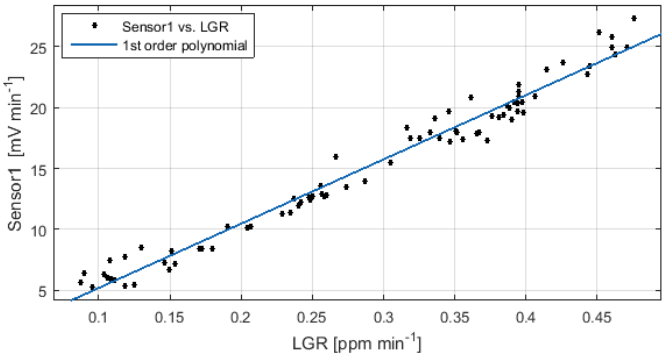

(a) $y = 52.81x - 0.094$ with R^2=0.97.

Sensor 1, 2nd order polynomial regression

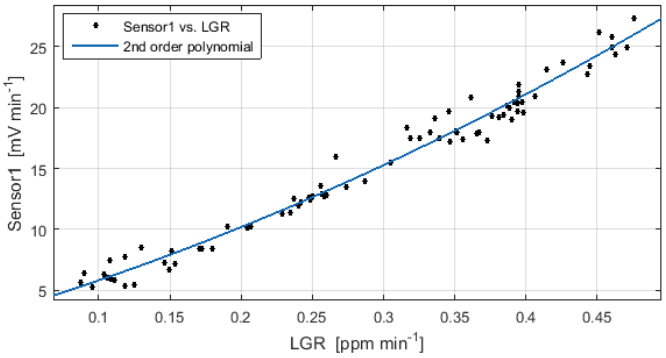

(b) $y = 36.41x^2 + 32.76x + 2.175$, R^2=0.98.

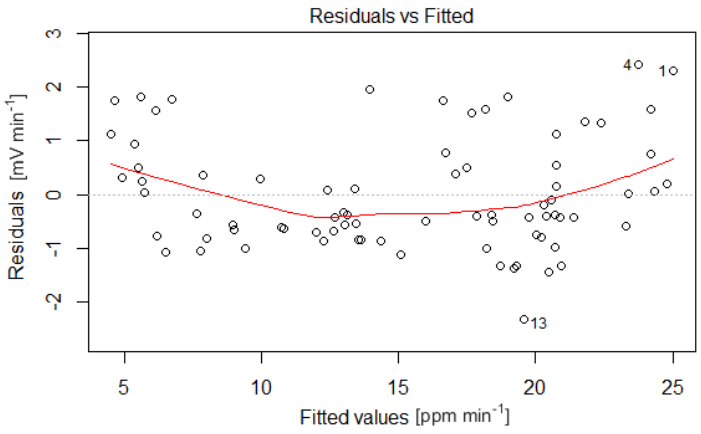

(c) Residuals versus fitted values

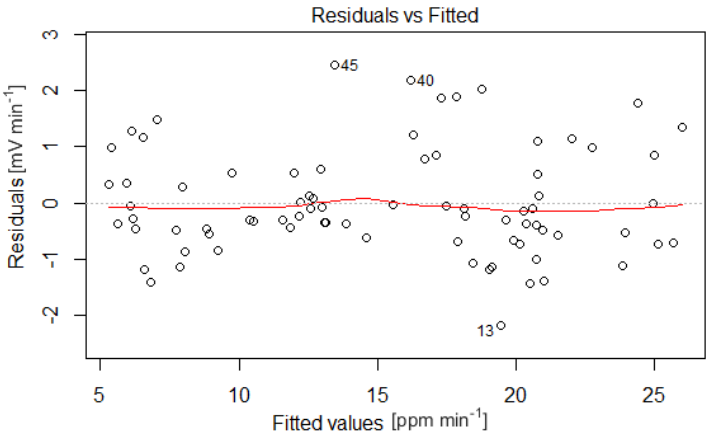

(d) Residuals versus fitted values

Figure 8: The results of the first and second order polynomial regressions of the Sensor 1, daily ΔRH-filtered data. The R^2-value improves slightly with the second order polynomial regression, and as seen in **(a)** and **(b)**, there is little difference between the two regression at this concentration range. The residuals display a more uniform spread under the second order regression.

Table 3: Summary of the flux data. Number of data points in brackets. All regressions had $p < 2.2 \cdot 10^{-16}$, indicating high significance. There was no significant difference between the regressions between the Figaro sensors versus the LGR.

	Sensor 1	**Sensor 2**	**Sensor 3**
Unfiltered data (9004)			
std_{res}	0.61	0.69	0.87
slope	47.91	28.50	23.04
intercept	2.78	1.80	1.75
R^2, 1st order	0.39	0.32	0.22
ΔRH-filter (8602)			
std_{res}	0.31	0.36	0.56
slope	47.87	28.67	22.71
intercept	1.4	0.81	0.94
R^2, 1st order	0.75	0.69	0.45
R^2, 2nd order	0.75	0.69	0.45
ANOVA (1st vs 2nd)	<<0.001	no sign.	<0.01
ΔRH-filter, daily (78)			
std_{res}	0.068	0.087	0.159
slope	52.81	31.11	25.87
intercept	0.094	-0.015	-0.15
R^2, 1st order	0.97	0.96	0.87
R^2, 2nd order	0.98	0.96	0.90
ANOVA (1st vs 2nd)	<0.001	<0.001	<0.001
Resolution [ppm]	0.0907	0.1565	0.1830

The regression and ANOVA results for the different chambers are presented in Table 3. The standard deviation of the standardized residuals (std_{res}) is used as an indication of the spread of the datasets. The spread decreases with the ΔRH-filtering and is lowest for Sensor 1, followed by Sensor 2 and 3 in all datasets. The R^2-values for the regressions of the unfiltered data were the following; 0.39 for Sensor 1, 0.32 for Sensor 2 and 0.22 Sensor 3. The slope of the regression line did not change much with the ΔRH-filtering, but the R^2-value increased to 0.75 for Sensor 1, 0.69 for Sensor 2 and 0.45 for Sensor 3.

The unfiltered data (9004 readings), ΔRH-filtered data (8602 readings) and ΔRH-filtered daily data (78 readings) datasets were assessed for the regression assumptions. The data is not normally distributed, due to the seasonal trend in the time series. The scatter plots of the raw data reveal a cluster of fluxes overestimated by the Figaro sensors compared to the LGR (Figure 6). The ΔRH-filter reduced the number of outliers and the daily ΔRH-filter data does not show any extreme outliers (Figure 6 and Figure 8(a)). Examination of the Q-Q plots (Figure A17, Appendix A) show how the data does not line up along the diagonal line, meaning that the residuals are not normally distributed around the regression line. There is less curvature in the Q-Q-plots for the daily data. Plots of residuals versus fitted values show a dense scatter for the large datasets, with the outliers clearly visible, but overall not much curvature in the trend (Figure A16, Appendix A). The daily data show more curvature in the trend, with higher residuals at low and high fitted values (Sensor 1, Figure 8(c)).

All the linear regression had p-values $<<$ 0.001, indicating very high significance. R^2 values improved with filtering and for the reduces daily mean data. Second order polynomial regressions also improve the R^2-values slightly (Sensor 1, Figure 8(b), and Sensor 2 Figure A18 and Sensor 3 Figure A20 in Appendix A). This regression reduce the curvature in the residual versus fitted plot (Figure 8(d)), particularly clear for Sensor 3 (Figure A20 in Appendix A).

The ANOVA between the regressions of the sensors show no significant difference. The ANOVA between the 1st and the 2nd order polynomial regression is significant for all three sensors using the daily data ($p<0.001$), but for the large ΔRH-filtered dataset only sensor 1 ($p<0.001$) and sensor 3 ($p<0.01$) were significant .

The concentration resolution, corresponding to the limitations of the analog-to-digital converter, is lowest for Sensor 1 and highest for Sensor 3. The daily ΔRH-filtered data produced slightly higher values, 0.091, 0.157 and 0.183 compared to 0.73, 0.142 and 0.174 for Sensor 1, 2 and 3 respective. The rank of the senors was the same for the two datasets.

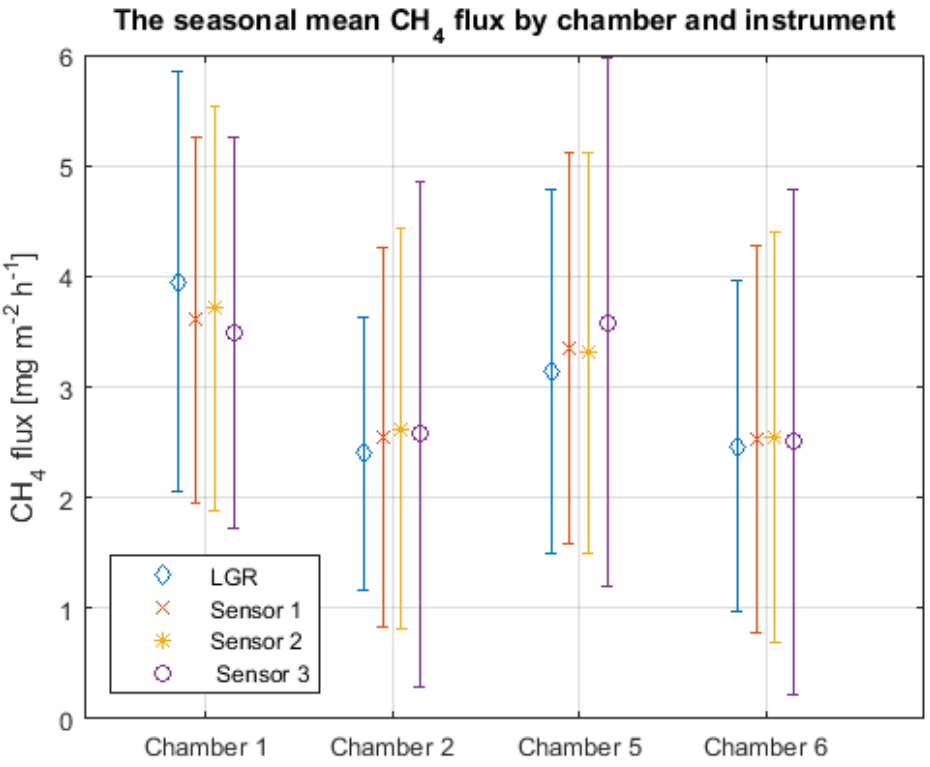

Figure 9: The seasonal mean fluxes for each chamber, by the different instruments. The results are from the ΔRH-filtered data and the sensors data is converted using the first order polynomial regression coefficients from the daily data. The variance between the chambers is larger than the difference between the instruments. The numbers are presented in Table 4.

Table 4: The seasonal mean flux [mg CH_4 m^{-2} h^{-1}] from each chamber by instrument. The mean flux from each sensor relative to the LGR (μ_i/μ_{LGR}) and the relative spread of the sensors compared to the LGR (std_i/std_{LGR}) is also presented.

	Chamber 1	Chamber 2	Chamber 3	Chamber 4	μ_i/μ_{LGR}	std_i/std_{LGR}
LGR	3.95	2.40	3.14	2.46	1	1
Sensor 1	3.61	2.54	3.35	2.53	1.006	1.100
Sensor 2	3.71	2.62	3.31	2.55	1.020	1.169
Sensor 3	3.49	2.57	3.58	2.50	1.017	1.392

The seasonal mean of the fluxes for each chamber for the LGR and the sensors are presented in Figure 9. The whiskers indicate the spread in the data calculated as the standard deviation. The sensors capture the magnitude of the LGR fluxes (Table 4). Larger differences are seen between the chambers than between the instruments. The full time series of the fluxes [mg m^{-2} h^{-1}] can be found in Figure 10.

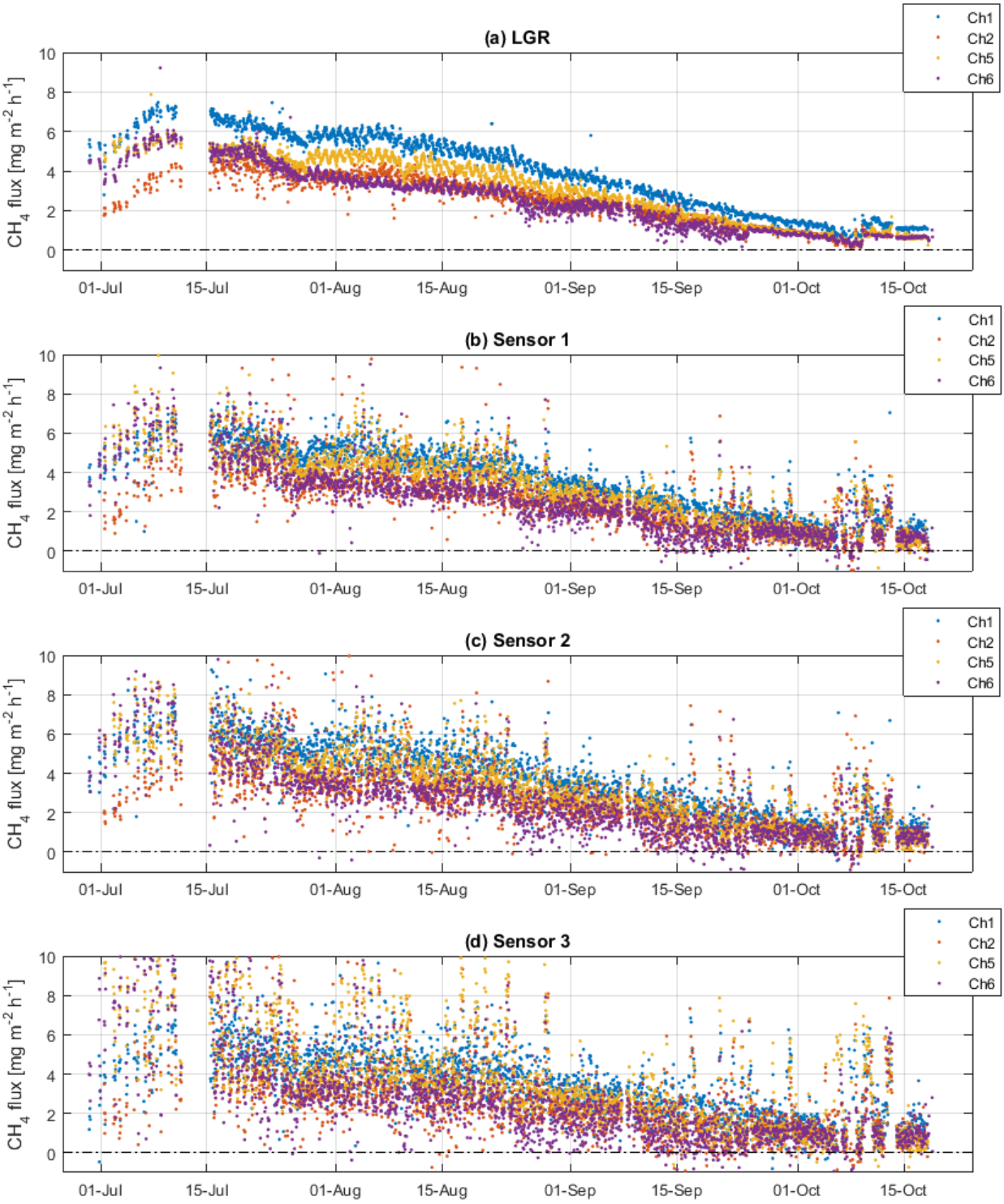

Figure 10: The seasonal CH_4 fluxes from the LGR and the Figaro sensors [mg m^{-2} h^{-1}], after applying the ΔRH-filter and converting the sensor data with the coefficients obtained by the first order polynomial regression of th daily data.

4.2 Relative humidity and temperature dependence

No patterns were found between bad data from the sensors and PAR, pressure or net radiation. The *Outlier*-filtered data presents a pattern of high temperatures and low humidity, both for air and soil, but no threshold values were identified (Figure 11). Outliers were typically found during afternoons, between 12 AM and 7 PM.

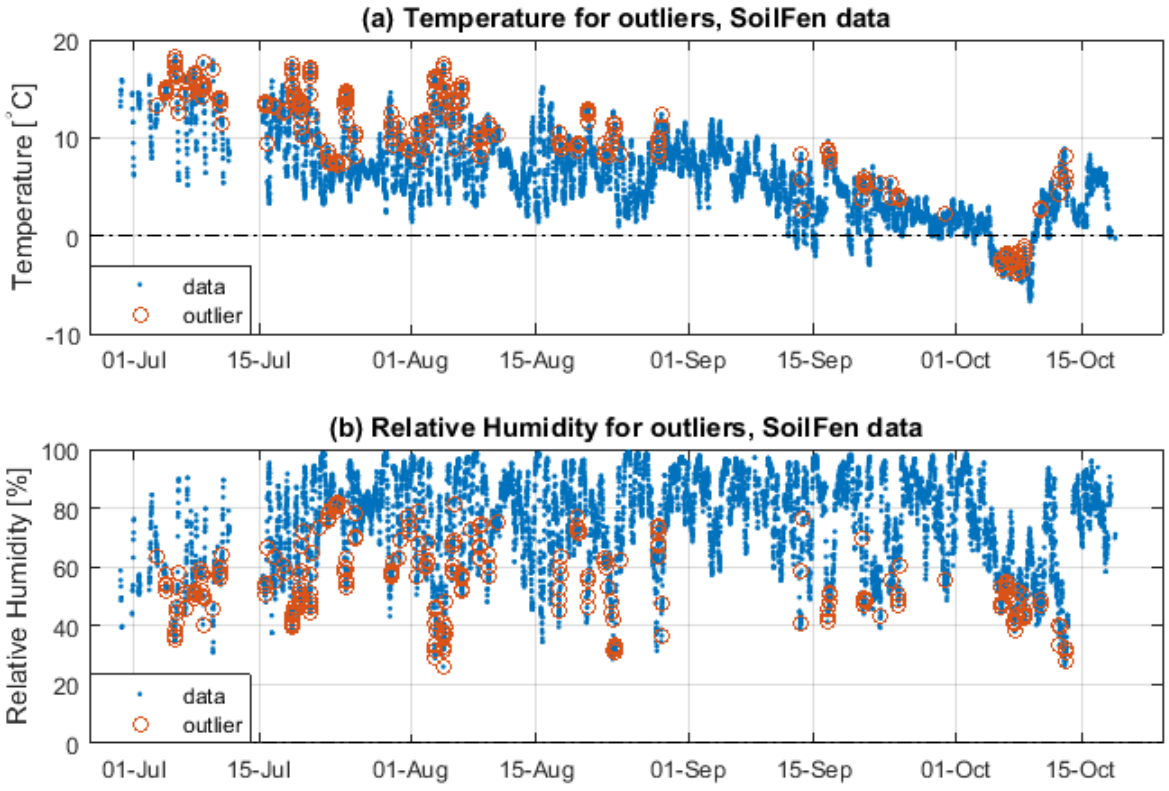

Figure 11: The general pattern of higher air temperatures **(a)** and low relative humidity **(b)** for overestimated sensor data, outliers, marked by orange circles. The unrepresentative outliers were obtained with the *Outlier*-filter for the Figaro sensor 1. 2.91% of the data was defined as outliers with this filter.

The temperature inside the syringe was constant on the temporal scale of individual flux calculations. The sensor temperature showed a larger daily variability than the outside air temperature. The temperature inside the syringe varied between 28℃ and 60℃, while the range of the air temperature was between -12℃ and 18℃, over the season. The temperature followed the same daily pattern as the air temperature measured by the SoilFen, but with a slight time lag (Figure 12). Drops in temperature around mid-day were seen on some days. The relative humidity was constantly lower in the syringe than outside (Figure 13), with a range of 7.2% and 55.0% compared to 26.1% and 99.6%.

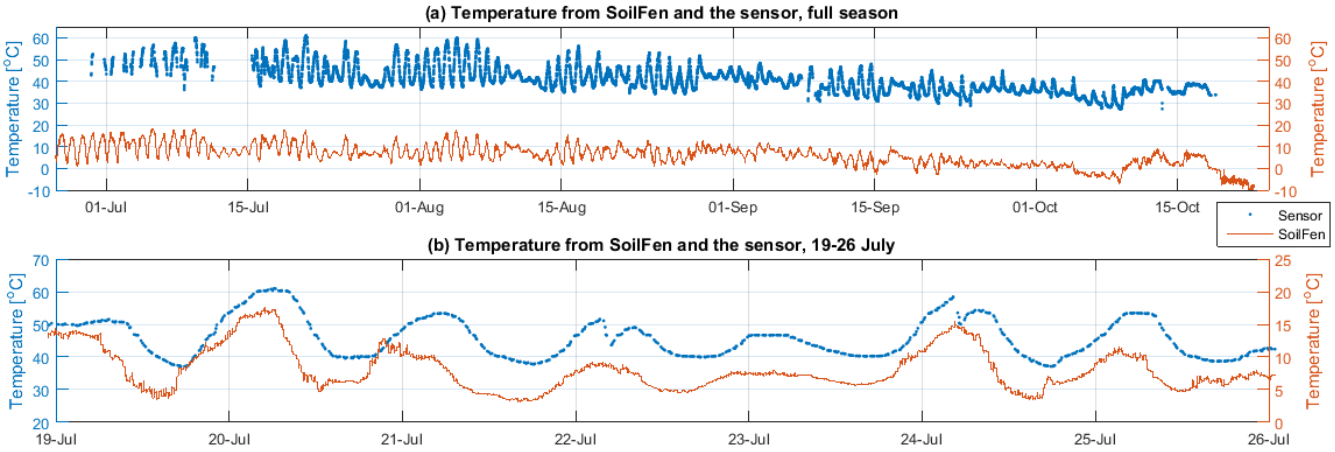

Figure 12: Air temperature from the SoilFen station and from the sensor inside the syringe. **(a)** shows the air temperature over the full season and **(b)** is zoomed in on a week in mid-July, with the yaxis changed to visualize the covariation in the air temperatures.

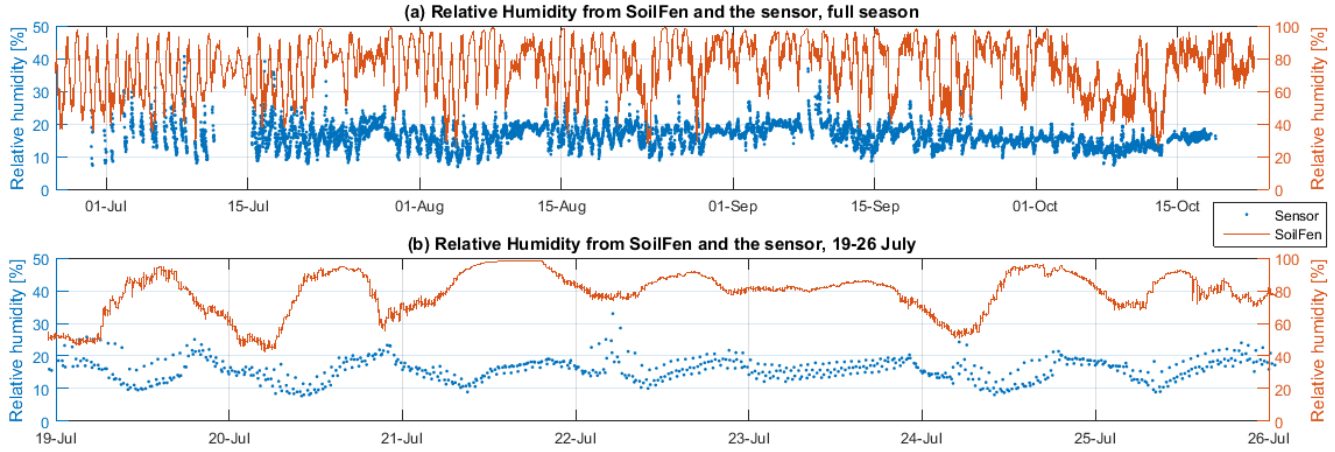

Figure 13: Relative humidity from the SoilFen station and from the sensor inside the syringe. **(a)** shows relative humidity over the full season and **(b)** is zoomed in on a week in mid-July. Note the different scales on the primary and secondary yaxis.

The relative humidity occasionally increased when a chamber closed. Figure 14 gives an example on two typical measurements, with similar LGR flux but differing relative humidity trend. One with stable relative humidity signal (Figure 14(a) and one when the relative humidity increases (Figure 14(b). This demonstrates how the sensor signal accompanies the relative humidity, and consequently increase more when the relative humidity rises. This rise in relative humidity was observed in combination with the overestimated fluxes, when processing the fluxes. Also during the last part of the season, around the freezing days, these rises in relative humidity coincided with the occurring overestimations. A second increase is visible in the sensors' signal by the end of the measurement(b), which is not seen in the LGR. At other times the relative humidity increased at first until it stabilized at a high value. The time with stable relative humidity was, at such times, used to calculate the flux. During the field work, there were observations of occasional condensation in the closed chambers.

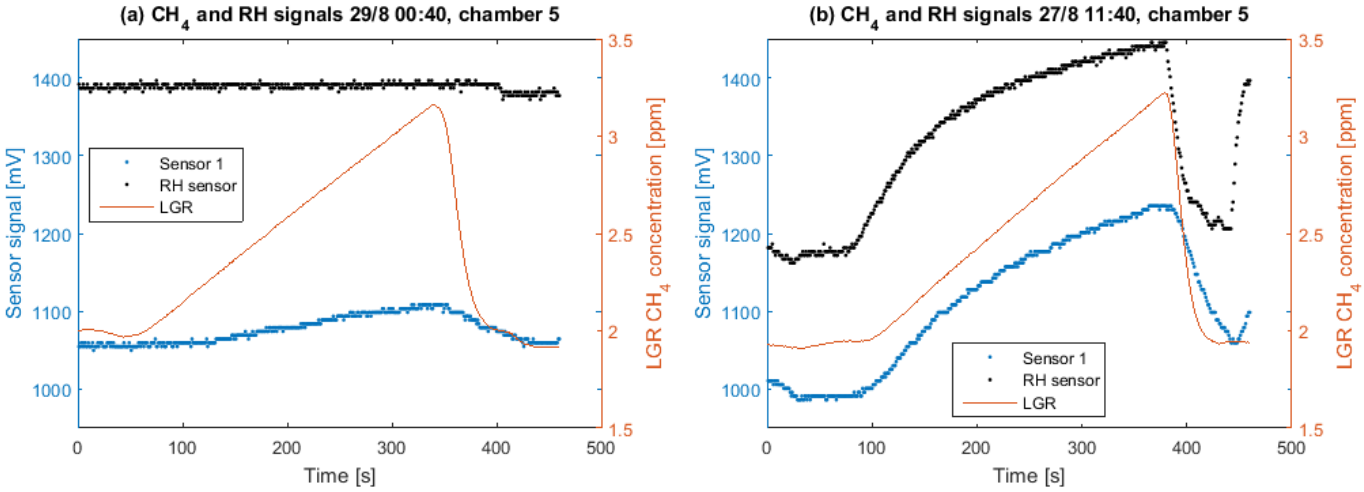

Figure 14: The signal from Sensor 1, the relative humidity sensor (RH sensor) and the LGR for two different days. (a) 29th of August at 00:40, with stable relative humidity signal, and (b) 27th of August at 11:40, when the relative humidity signal increases. Both measurements are from chamber 5. The air temperature was stable during both measurements.

The coefficients from the different measurements did not match and the attempts to find a model correcting for relative humidity and temperature were unsuccessful. The post-field laboratory test showed how the sensors signal behaved unreliably at low relative humidity. The syringe accidentally got water-filled during the tests and the sensors broke before more thorough tests could be conducted.

5 Discussion

5.1 Seasonal patterns in the CH_4 fluxes

The objective of this study was to make a technical assessment of the three Figaro sensors, therefore the more commonly used flux unit [mg CH_4 m^{-2} h^{-1}] was calculated only as a final step. The main reason was to reduce the error from an extra conversion. Since the extreme outliers could have a large influence, the strength of the regressions were assessed before the regression equations were used to convert sensor fluxes from [mV min^{-1}] to [ppm min^{-1}] and the data was presented in its output unit throughout most of the analysis. In equation (3), the output voltage is linearly dependent on the CH_4 concentration, assuming a linear response between resistance and concentration (α=1, equation (1)). The clean air resistance, R_0, of the sensors, was not measured in advance, and proved to be difficult to obtain since dry calibration gases could not be used. With the setup used in this study and by measuring the concentration change rather than the absolute concentration, the voltage served well as a proxy for CH_4 concentration.

The seasonal pattern in the Kobbefjord CH_4 fluxes looks rather different compared to earlier years CH_4 fluxes, e.g. Hansen et al. (2013, 2014). This is likely due to the late onset of the growing season. Large amount of snow remained at the fen until late June. Due to additional technical issues the chamber measurements did not start until the 27th of June. It meant that the emission onset was not recorded. The flux data show a drastic increase the first couple of weeks, with a peak on the 8th of July, which is quite early, compared to previous years. Christensen et al. (2012) observed emissions by the start of snow-melt, despite the presence of snow. It would hence be preferred to start the measurements before snow melt has completed.

From a visual assessment, the Figaro sensors appear to capture the 2015 seasonal trend of CH_4 fluxes in Kobbefjord. They reproduce rising fluxes at the start of the season that diminish throughout the season. A small increase in fluxes is seen by the end of the season, right after a few days of freezing temperatures. The soil thermometers show that only a few cm of soil froze and the little burst came as it started to thaw again. This is expected to be accumulated CH_4 produced at greater depths when the frozen top soil prevent emissions, and release as the top soil layer thawed. The sensors record overestimated fluxes related to those freezing days. Further assessment should try to understand the reason behind these overestimations, to conclude whether the sensors could be used on a year round basis. For use of sensors in permafrost regions, reliable performance during freezing conditions are important to detect potential autumn bursts (Mastepanov et al., 2008, 2013; Pirk et al., 2015b).

The overall scatter in the sensor data is considerably larger, and the signal less clear, than for the LGR. The sensors were not expected to be as good as, or better than, the LGR. Instead they would provide a cheaper alternative for primarily assessments of CH_4 fluxes, while more precise studies would be performed with more precise instruments. The scatter plots show the covariation between sensors and LGR and the majority of the data indicate a linear relationship. To understand how reliable the regressions are, the data was analyzed to see how well it fulfilled the regression assumptions.

The first drawback is that the data is not normally distributed, due to the seasonality. The standard deviation of the standardized residuals is therefore not quite appropriate, or accurately used, but here it serves the purpose of assessing the relative spread in the different datasets. A seasonal trend causes autocorrelation in these data; with a previous

high value the next value is more likely to also be high. There are different levels of autocorrelation in this data; the seasonal trend, the daily patterns, but also the differing magnitudes of the chambers. Ideally, the seasonal trend should be removed, to potentially obtain normally distributed data. Removal of the seasonal autocorrelation requires advanced time series analysis, which is beyond the scope of this project. As discussed in Mastepanov et al. (2013) statistical test and regressions could be of descriptive use, even if the applicability could be questionable. Autocorrelation of the residuals would not necessarily be present in the time series data, if it was not for the outlier regions; prevailing conditions causing outliers makes it more probable that also the following reading will be an outlier. The extreme outliers present in the large datasets can have a big influence on the regressions. The daily data does, as expected, not show any extreme outliers.

The quantile-quantile (Q-Q) plots of the large data sets show strong deviations from normality in the residuals. In a Q-Q plot the ordered observed standardized residuals are plotted against the ordered theoretical standardized residuals that would occur with normally distributed residuals. Even if the performance improve with the daily means, some curvature is still left. Curvature is also seen in the residuals versus fitted values plot for the daily data. This indicates non-linearity in the relationship. Therefore the second order polynomial regressions were tested.

The R^2-values of the different regressions are very similar, but the second order polynomial regression has less curvature in the residual versus fitted plot, thus better homoscedasticity. This means that the errors are more evenly spread through the data. The ANOVA-test indicates a significant difference between the two types of regressions. There is a potential risk of type 1 error, finding significance when there is none, due to violated regression assumptions. For better statistical certainty further tests with more sensor replicas should be performed. If the second order polynomial regression is better, as the ANOVA-test suggests, α=2 should be used in equation (1) to describe the sensors' sensitivity to CH_4. Disputing this result is the higher intercept of the second order polynomial regressions. A flux of zero, should be zero for both the LGR and the Figaro sensors, which means that the regression line should go through [0,0]. With the flux range in this project, differences between the two regressions are relatively small (Figure 8). According to the principle of parsimony (to choose the simplest alternative that accounts for the facts) the first order polynomial regression is therefore used for the conversion.

Since there are some shortcomings in the data, related to the linear regression assumption attention should be taken when drawing conclusions based on these. All the regressions have very low p-values, indicating high significance. Low p-values can be expected for such large datasets though, and there is again a risk of type 1 error; to obtain significance where there is none. Tagesson et al. (2012) dealt with violated assumptions in their data, due to seasonality, by only presenting R^2-value, and not p-values, and emphasize the added difficulties on making conclusions based on such data. In this project, I take similar actions, by analyzing the data primarily in a descriptive way and be careful regarding the strength of my conclusions.

Most of the extreme outliers could be identified by when the relative humidity changed more than 50 mV, corresponding to 27%. This improved the R^2-value means that more of the variation in the sensor fluxes could be explained by the LGR, thus the real CH_4 fluxes. The ΔRH-filtering does not affect the slope of the regression line much, but the intercept, which got closer to zero. Since the filter compare the maximum to minimum relative humidity it also identifies corresponding drops in relative humidity. Consequently,

this filter identifies both over- and underestimations. In the flux calculations the time interval was set to when the relative humidity is as constant as possible. This was done to get as accurate data as possible, but meant that all these large RH changes are not identified, which could explain some of the remaining outliers. The threshold value was chosen by a visual assessment of the value identifying maximum number of outliers without the expense of other data. A more analytic approach could be developed to find the best ΔRH-threshold. Chamber 2 accounts for the majority of the ΔRH$\geq$50-occurrences. Since this project was not set up to analyze the differences between the chambers, and controls of CH_4 fluxes at this site, data to explain this difference is not available. By analyzing the chambers' conditions, e.g. water table depth, humidity and vegetation, the understanding of what is producing these conditions could be improved.

The time period, 15th of July to 30th of September, used for the daily means, is chosen for several reasons. It represents the time with the temporally most continuous data, and excludes the large fluctuations during the freezing days in October. The daily mean removes diurnal fluctuations and also has the potential to cancel out errors. The daily values are calculated based on the ΔRH-filtered data. Consequently, some means are calculated from fewer fluxes. The LGR show how fluxes are higher during daytime, and the outliers mostly occurred then. The filtered days could thus have reduce mean values, and affect the regression analysis. The purpose of this dataset is to obtain the clearest relationship between the LGR and the sensors, and a reliable conversion equation. The R^2-value is the highest for this dataset, and the data fulfilled the regression assumptions better. Hence, this regression is assumed to be the most reliable, and is therefore used to convert the data from [mV] to [ppm min^{-1}].

Some of the uncertainty in the sensor data should be accredited to the procedure with which fluxes are calculated. With this setup, the resolution of sensor data is not limited by the sensor itself, but the analogue-to-digital converter. The concentration change is resolved but in a step-like manner, compared to the more continuous increase in LGR concentration. This makes the flux calculation more sensitive to the choice of time interval. An un-quantified part of the observed spread can be due to the converter, and can thus be improved. Better resolution would make it easier to identify the most linear part of the concentration curve. The software DataShow should incorporate the sensors data and automatically choose the most linear part to give a more objective result.

Sensor 1 has the highest voltage output. As mentioned, such characteristics are highly individual and differ between sensors, also of the same type. In this setup, with the limiting converter resolution, high voltage range per CH_4 change is favorable. This is reflected in the calculated resolutions, which is about two times better for Sensor 1 compared to Sensor 3. Sensor 1 performed better throughout the analysis, e.g. lower spread and higher R^2-values, but this result can not be statistically supported. It is therefore suggested that the sensors should be tested with more replicas of each. This would enable both testing statistically and assessment of different sensors of the same type.

Seasonal mean fluxes similar to the LGR fluxes are reproduced when applying the ΔRH-filtering and converting the fluxes with the regression coefficients reproduces. The variance between the chambers is larger than the difference between the instruments. The total mean fluxes from the chamber lie within a few percent deviation from the LGR mean, 0.6%, 2.0% and 1.7% for Sensor 1, 2 and 3 respectively. The spread in the data is 10%, 17% and 39% higher than the LGR, for the sensors respectively. This gives an indication that these sensors could be used to detect differences in CH_4 emissions,

although this could not be statistically supported a consequence of the lack of replicas, and the presence of the seasonal trend.

5.2 Relative humidity and temperature dependence

The *Outlier*-filter threshold is chosen in a way which identified the apparent outliers, but that also could be applied to all sensors with their various magnitudes. A more analytic way of obtaining this threshold could be to find the value which identified data with a Cook's d-value higher than accepted.

The outliers come in little bursts, mostly during afternoons of warm and dry days. This indicates that there is a specific cause for these outliers and they are not just bad readings by the sensors. As mentioned by the manufacturer and shown in earlier studies, the sensors are sensitive to relative humidity and temperature (Figaro USA Inc., 2005a; Eugster and Kling, 2012). Eugster and Kling (2012) measured concentration changes in the open air to estimate fluxes from surrounding areas. Their setup is more sensitive to fluctuations in air temperature and relative humidity, and also requires higher resolution to resolve the small concentration changes.

The changes in relative humidity measured in the sensor syringe are not seen in the atmospheric data and must be an artifact of the chambers. Since the temperature was stable under each individual measurement, the rise in relative humidity is an effect of changing water vapor content in the air, the absolute humidity. When a chamber closes, water evaporating from the soil will cause the relative humidity to rise. If the relative humidity reaches 100%, further evaporation will cause condensation, which was observed occasionally. Such conditions are probably what cause the relative humidity to stabilize at a high value. Under those circumstances the stable part by the end of the measurement was used to calculate the flux, and the obtained data would hopefully be an accurate representation. If saturation is not reached, the concentration increase continues without stabilizing, which causes overestimated fluxes (Figure 14). Available latent heat flux data from the eddy covariance did not have high enough temporal resolution for analysis in this project, but could potentially describe the conditions behind the relative humidity rise. The sensors did not perform well around the cycles of freezing and succeeding little bursts. Also at these times the overestimated fluxes could be accredited to rising relative humidity during the measurement.

The measurement in Figure 14(b) shows an unexpected increase in relative humidity and sensors signal by the end of the measurement, a change which is not seen in the LGR and occurs when the chamber is open. The reason behind this rise in relative humidity rise is unknown, but since this is outside the measurement period, it does not affect the flux calculation itself. The signal does not recover to its initial level, as seen in the figure, which could be problematic. The sensors are known to take longer time to recover than to react. The time schedule is developed for the system to get properly flushed out between measurements from the different chambers and should, under stable conditions, give instruments enough time to recover. Unexpected changes during the recovery period, e.g. relative humidity increase, could mean that the signal has not stabilized when the next measurement starts. The following flux calculation would then be inaccurate. This potential error is not properly assessed in this study, and should be further investigated.

The relative humidity was lower inside the sensor syringe compared to ambient conditions, which can have several causes. The higher temperature in the syringe makes the relative humidity lower by definition, as warm air can hold more water vapor. Condensa-

tion could occur in the tubes going from the chambers to the instruments, which means that the absolute humidity decreases. The initial idea to find a model for the concentration's dependence on relative humidity and temperature proved to be of a complexity beyond the scope of this project. As seen in previous studies, low relative humidity affects the response of the sensors. Eugster and Kling (2012) excluded data with relative humidity below 40% from the analysis. The post-field laboratory tests of the sensors support this unreliable behavior at low relative humidity. Laboratory tests and calibration are complicated by the relative humidity sensitivity, which means that standard gases cannot be used. Out of the data 99.5% is below 30% relative humidity, which would explain the difficulty of fitting a model. Coefficients were obtained for individual measurements but could not be generalized. A more complex relationship may be needed to describe the behavior of the data at low relative humidity. It would be more accurate to correct the sensor signal for absolute humidity, since it is the number of water vapor molecules that affects the resistance. If the signal is corrected for relative humidity and temperature, the temperature will have a double effect; both direct by affecting the rate of chemical reactions and indirectly via the relative humidity. More advanced corrections of the sensors' signals are outside the scope of this project, and the focus was set on finding the conditions under which the Figaro sensors produced valid data, without corrections.

Sensor temperature was noticeably higher than the air temperature. The padded cardboard box probably had an insulating effect, which combined with the sensor heaters caused the temperature inside the syringe to increase. Also, the wooden box with the Zarges box, containing all instruments, warmed up, especially on sunny summer days. The slight time lag in the sensor temperature compared to air temperature is expected to be an effect of the time it takes to heat up or cool down the Zarges box. The little drops in temperature that are seen on some days could potentially be the ventilating effect by opening of the box. The manufacturer does not present how the sensors responds to temperatures above 40℃ (Figaro USA Inc., 2005a). The effect from the high temperatures prevailing in this study should be further examined. The concentration's dependence on temperature was not evaluated in this thesis but should not be disregarded.

No indications of other compounds, e.g. CO or ethanol, were seen. Sensor 1 is sensitive to several other gases, while sensor 2 and 3 primarily are primarily sensitive to CH_4. If other deoxidizing gases were present deviations between the sensors signals could be expected, which was not seen in this study. Such compounds could be present at other sites, e.g. Bäckstrand et al. (2008) found significant contributions of non-methane volatile organic compounds from a subarctic mire in Abisko, northern Sweden. For use at such sites, the more CH_4 specific sensors (sensor 2 and 3) are expected to be suitable.

The drift in the sensor signal over the season was not assessed in this study. This could be done by comparing the atmospheric CH_4 concentration from the sensors to the LGR over the course of the season, but require corrections for temperature and relative humidity. Measurements of concentration change are less sensitive to eventual drift, compared to absolute concentration, but the effect should still be assessed. Also left out of this study, was the potential effect of initial action, explained in Section 3.2. According to the manufacturer the resistance drops sharply when the sensors are turned on and slowly recovers over a time frame depending on the "storage time" (Figaro USA Inc., 2012a). Initial action could have an impact on the first few measurements after a larger power shortage.

5.3 Outlook

By using the low-cost alternatives, such as the Figaro sensors, for CH_4 flux measurements, requested extensive monitoring networks could be developed throughout the Arctic region (Christensen, 2014), since the reduced cost enables more replicas. Lower power consumption means that small solar panels could provide electricity even late in the season, when the insolation is low. Additionally, the small size opens up for creative new setup alternatives.

Each sensor has to be calibrated against a reliable instrument, as they all have their individual characteristics. Calibration at the start and end of the season should capture eventual signal drift. Additional analysis should test how stable the calibration coefficients are; if they change over time, with transportation, after storage etc, even if the manufacturer states that the characteristics are stable over time Figaro USA Inc. (2005a).

Further tests of the sensors are needed; with more replicas and at several sites of various conditions. In this study, only a few percent of the data was filtered out due to unfavorable conditions, but these conditions could be more problematic at other sites. I suggest to focus on understanding the sensors' response to absolute humidity and temperature. Since the humidity sensitivity is due to the number of water molecules, absolute humidity should be assessed instead of the relative humidity. Alternative setups could be used to avoid the problems caused by the humidity sensitivity, although keeping an automatic setup is of value to capture episodic responses that otherwise could be missed (Petrescu et al., 2015). If sensors were placed inside the chambers the low humidity problem could most likely be solved. The chances of obtaining a model describing a humidity dependence is likely to improve with relative humidity above 40%.

Finding a way of correcting for such dependencies is of prominent importance for year round measurements, since humidity rises caused unstable signal associated with freezing. Several studies indicate the importance of full year measurements of CH_4 emissions, to understand the temporal variability (McGuire et al., 2009; Mastepanov et al., 2013). For full year measurements the automatic chamber method cannot be used, since snow can prevent lids from closing and burying outlet tubes, or sensors. Absolute concentration measurements in the open air provides information on larger spatial scales, but has higher requirements on sensor resolution and is more sensitive to changes in ambient conditions. Also the sensors' response time must be considered for such techniques. There is space for new creative ideas of how to measure CH_4 fluxes on a year round basis, using the Figaro sensors.

6 Conclusions

The objective of this study was to compare the data from the three Figaro sensors to the reliable LGR instruments, in order to test how well the sensors could distinguish patterns in CH_4 fluxes. The linear relationship between the Figaro sensors and the reliable LGR instrument provided mean seasonal fluxes within a few percent deviation from the LGR. Also the varying magnitude of the chambers was resolved on a seasonal scale. These results could not be statistically supported due to lack of replicas and presence of seasonality in the data. Seasonal patterns were visually distinguished in the time series, although the spread was noticeably higher than for the LGR. Much of the spread is expected to be due to limitations in resolution from the analog-to-digital converter, and the manually chosen intervals for the flux calculation. In this setup the sensors provide means of measuring general trends in the CH_4 fluxes, but not smaller variation on e.g. diurnal scales.

The sensors' sensitivity to humidity and temperature has to be considered. In this setup the largest effect was due to changes in relative humidity as an artifact of the chambers, which produced erroneous fluxes. By filtering out data with changes in relative humidity higher than 27%, the performance improved. The attempt of finding a model describing the sensors' dependence of relative humidity and temperature was unsuccessful. The failure was most likely a result of the low relative humidity inside the syringe, containing the sensors. Previous studies have shown how these sensors change behavior in low relative humidity (Eugster and Kling, 2012). These relative humidity changes, related to ambient high temperatures and low relative humidity, could be avoided by changing the measurement setup and placing the sensors within each chamber.

Sensor 1 showed the best performance, but no conclusion of which of the sensors that perform the best could be made, as a consequence of the limited resolution. Further testing of the sensors with several replicas and under various conditions are needed, as a consequence of the individual characteristics of each sensors and the potential effect from deoxidizing gases at other sites.

With some refinements, these sensors may well be used in a future monitoring network covering a diverse range of potential CH_4 emitting sites. This has the potential to significantly improve the understanding of spatial and temporal variability in CH_4 emissions as well as processes governing these, an important contribution to reduce the uncertainty related to the Arctic region in a warming climate.

Acknowledgments

First of all, I want to thank my supervisors, Mikhail Mastepanov and Torben R. Christensen, for introducing me to the project, and their great support and enthusiasm throughout my work. Thanks to Magnus Lund for support during the field work, and providing data. Further, I want to thank Efrén López Blanco for being such a great field work companion. Acknowledgments to the Nuuk Ecological Research Operations, GeoBasis team, for a great field work sites, providing data and helpful field work colleges; Maria Libach, Maia Olsen, Katrine Raundrup and Daniel Alexander Rudd. Benjamin Claréus, I am so thankful for all the statistics support, your patience and for taking the time to explain, over and over again! Finally, great thanks to friends and family for feedback on my work, and support through the process.

References

Bäckstrand, K., Crill, P. M., Jackowicz-Korczyñski, M., Mastepanov, M., Christensen, T. R., and Bastviken, D. (2010). Annual carbon gas budget for a subarctic peatland, northern sweden. *Biogeosciences*, 7(1):95–108.

Bäckstrand, K., Crill, P. M., Mastepanov, M., Christensen, T. R., and Bastviken, D. (2008). Non-methane volatile organic compound flux from a subarctic mire in Northern Sweden. *Tellus, Series B: Chemical and Physical Meteorology*, 60 B(2):226–237.

Bay, C., Aastrup, P., and Nymand, J. (2008). The NERO line. A vegetation transect in Kobbefjord, West Greenland. Technical Report 693, National Environmental Research Institute, University of Aarhus, Denmark.

Blake, L. I., Tveit, A., Øvreås, L., Head, I. M., and Gray, N. D. (2015). Response of Methanogens in Arctic Sediments to Temperature and Methanogenic Substrate Availability. *PLoS ONE*, 10(6):e0129733.

Christensen, J., Kumar, K. K., Aldria, E., An, S.-I., Cavalcanti, I., Castro, M. D., Dong, W., Goswami, P., Hall, A., Kanyanga, J., Kitoh, A., Kossin, J., Lau, N.-C., Renwick, J., Stephenson, D., Xie, S.-P., and Zhou, T. (2013). Climate Phenomena and their Relevance for Future Regional Climate Change Supplementary Material. In *Climate Change 2013: The Physical Science Basis. Contribution of Working Group I to the Fifth Assessment Report of the Intergovernmental Panel on Climate Change*, pages 1217–1308. [Stocker, T.F., D. Qin, G.-K. Plattner, M. Tignor, S.K. Allen, J. Boschung, A. Nauels, Y. Xia, V. Bex and P.M. Midgley (eds.)]. Cambridge University Press, Cambridge, United Kingdom and New York, NY, USA.

Christensen, T., Jackowicz-Korczyński, M., Aurela, M., Crill, P., Heliasz, M., Mastepanov, M., and Friborg, T. (2012). Monitoring the Multi-Year Carbon Balance of a Subarctic Palsa Mire with Micrometeorological Techniques. *AMBIO: A Journal of the Human Environment*, 41(Supplement 3):207–217.

Christensen, T. R. (2014). Understand Arctic methane variability. *Nature*, 509:279–281.

Ciais, P., Sabine, C., Bala, G., Bopp, L., Brovkin, V., Canadell, J., Chhabra, A., DeFries, R., Galloway, J., Heimann, M., Jones, C., Quéré, C. L., Myneni, R., Piao, S., and Thornton, P. (2013). Carbon and Other Biogeochemical Cycles. In *Climate Change 2013: The Physical Science Basis. Contribution of Working Group I to the Fifth Assessment Report of the Intergovernmental Panel on Climate Change*, pages 465–570. [Stocker, T.F., D. Qin, G.-K. Plattner, M. Tignor, S.K. Allen, J. Boschung, A. Nauels, Y. Xia, V. Bex and P.M. Midgley (eds.)] Cambridge University Press, Cambridge, United Kingdom and New York, NY, USA.

Erich, M., Goosse, H., Lucas, C., and Morice, C. (2013). Long-term Climate Change: Projections, Commitments and Irreversibility. In *Climate Change 2013: The Physical Science Basis. Contribution of Working Group I to the Fifth Assessment Report of the Intergovernmental Panel on Climate Change*, pages 1029–1136. [Stocker, T.F., D. Qin, G.-K. Plattner, M. Tignor, S.K. Allen, J. Boschung, A. Nauels, Y. Xia, V. Bex and P.M. Midgley (eds.)] Cambridge University Press, Cambridge, United Kingdom and New York, NY, USA.

Eugster, W. and Kling, G. W. (2012). Performance of a low-cost methane sensor for ambient concentration measurements in preliminary studies. *Atmospheric Measurement Techniques*, 5(8):1925–1934.

Field, C., Barros, V., Mach, K., Mastrandrea, M., van Aalst, M., Adger, W., Arent, D., Barnett, J., Betts, R., Bilir, T., Birkmann, J., Carmin, J., Chadee, D., Challinor, A., Chatterjee, M., Cramer, W., Davidson, D., Estrada, Y., Gattuso, J.-P., Hijioka, Y., Hoegh-Guldberg, O., Huang, H., Insarov, G., Jones, R., Kovats, R., Romero-Lankao, P., Larsen, J., Losada, I., Marengo, J., McLean, R., Mearns, L., Mechler, R., Morton, J., Niang, I., Oki, T., Olwoch, J., Opondo, M., Poloczanska, E., Pörtner, H.-O., Redsteer, M., Reisinger, A., Revi, A., Schmidt, D., Shaw, M., Solecki, W., Stone, D., Stone, J., Strzepek, K., Suarez, A., Tschakert, P., Valentini, R., Vicuña, S., Villamizar, A., Vincent, K., Warren, R., White, L., Wilbanks, T., Wong, P., and Yohe, G. (2014). Technical summary. In: Climate Change 2014: Impacts, Adaptation, and Vulnerability. Part A: Global and Sectoral Aspects. Contribution of Working Group II to the Fifth Assessment Report of the Intergovernmental Panel on Climate Change. In *Climate Change 2014: Impacts, Adaptation, and Vulnerability. Part A: Global and Sectoral Aspects. Contribution of Working Group II to the Fifth Assessment Report of the Intergovernmental Panel on Climate Change*, pages 35–94. [Field, C.B., V.R. Barros, D.J. Dokken, K.J. Mach, M.D. Mastrandrea, T.E. Bilir, M. Chatterjee, K.L. Ebi, Y.O. Estrada, R.C. Genova, B. Girma, E.S. Kissel, A.N. Levy, S. MacCracken, P.R. Mastrandrea, and L.L. White (eds.)]. Cambridge University Press, Cambridge, United Kingdom and New York, NY, USA.

Figaro USA Inc. (2005a). Technical Information on Usage of TGS Sensors for Toxic and Explosive Gas Leak Detectors. `http://www.figarosensor.com/products/common(1104).pdf`. Accessed: 2016-05-20.

Figaro USA Inc. (2005b). TGS 2600 - for the detection of Air Contaminants. `http://www.figarosensor.com/products/2600pdf.pdf`. Accessed: 2016-05-20.

Figaro USA Inc. (2012a). Technical Information for TGS2600: Technical Information for Air Quality Control Sensors. `http://www.figarosensor.com/products/2600Dtl.pdf`. Accessed: 2016-05-20.

Figaro USA Inc. (2012b). Technical Information for TGS2611: Technical Information for Methane Gas Sensors. `http://www.figarosensor.com/products/2611Dtl.pdf`. Accessed: 2016-05-20.

Figaro USA Inc. (2013). TGS 2611 - for the detection of Methane. `http://www.figarosensor.com/products/2611pdf.pdf`. Accessed: 2016-05-20.

GEMdatabase (2016). Greeland ecosystem monitoring database. `http://data.g-e-m.dk/`. (Accessed: 2016-05-24).

Hansen, B. U., Christensen, L. H., Tamstorf, M. P., Lund, M., Højlund Pedersen, S., Libach Burup, M., Raundrup, K., Mastepanov, M., Westergaard, A., and Christensen, T. R. (2014). Nuuk basic: The geobasic programme. In *Nuuk Ecological Research Operations, 7 th Annual Report*, chapter 3. [Jensen, L. M. and Christensen, T. R. (eds.)] Aarhus University, DCE - Danish Centre for Environment and Energy.

Hansen, B. U., Christensen, L. H., Tamstorf, M. P., Lund, M., Højlund Pedersen, S., Libach Burup, M., Raundrup, K., Mastepanov, M., Westergaard-Nielsen, A., and Christensen, T. R. (2013). Nuuk basic: The geobasic programme. In *Nuuk Ecological Research Operations, 7 th Annual Report*, chapter 3. [Jensen, L. M. and Rasch, M. (eds.)] Aarhus University, DCE - Danish Centre for Environment and Energy.

Hayes, D. J., Kicklighter, D. W., McGuire, a. D., Chen, M., Zhuang, Q., Yuan, F., Melillo, J. M., and Wullschleger, S. D. (2014). The impacts of recent permafrost thaw on land–atmosphere greenhouse gas exchange. *Environmental Research Letters*, 9(4):045005.

Hope, C. and Schaefer, K. (2015). Economic impacts of carbon dioxide and methane released from thawing permafrost. *Nature Climate Change*, 403(September):1–6.

Jackowicz-Korczyński, M., Christensen, T. R., Bäckstrand, K., Crill, P., Friborg, T., Mastepanov, M., and Ström, L. (2010). Annual cycle of methane emission from a subarctic peatland. *Journal of Geophysical Research*, 115(G2):1–10.

Johansson, M., Callaghan, T. V., Bosiö, J., Åkerman, H. J., Jackowicz-Korczynski, M., and Christensen, T. R. (2013). Rapid responses of permafrost and vegetation to experimentally increased snow cover in sub-arctic Sweden. *Environmental Research Letters*, 8(3):035025.

Juszczak, R. (2013). Biases in methane chamber measurements in peatlands. *International Agrophysics*, 27:159–168.

Mastepanov, M. (2009). CH4 and CO2 flux monitoring system Operator's manual 2009 (Nuuk). page 24 pp.

Mastepanov, M., Sigsgaard, C., Dlugokencky, E. J., Houweling, S., Ström, L., Tamstorf, M. P., and Christensen, T. R. (2008). Large tundra methane burst during onset of freezing. *Nature*, 456(7222):628–30.

Mastepanov, M., Sigsgaard, C., Tagesson, T., Ström, L., Tamstorf, M. P., Lund, M., and Christensen, T. R. (2013). Revisiting factors controlling methane emissions from high-Arctic tundra. *Biogeosciences*, 10(7):5139–5158.

McGuire, A. D., Anderson, L. G., Christensen, T. R., Dallimore, S., Guo, L., Hayes, D. J., Heimann, M., Lorenson, T. D., Macdonald, R. W., and Roulet, N. (2009). Sensitivity of the carbon cycle in the Arctic to climate change. *Ecological Monographs*, 79(4):523–555.

McGuire, A. D., Chapin, F., Walsh, J. E., and Wirth, C. (2006). Integrated Regional Changes in Arctic Climate Feedbacks: Implications for the Global Climate System. *Annual Review of Environment and Resources*, 31(1):61–91.

Myhre, G., Shindell, D., Bréon, F.-M., Collins, W., Fuglestvedt, J., Huang, J., Koch, D., Lamarque, J.-F., Lee, D., Mendoza, B., Nakajima, T., Robock, a., Stephens, G., Takemura, T., and Zhan, H. (2013). Anthropogenic and Natural Radiative Forcing. In *Climate Change 2013: The Physical Science Basis. Contribution of Working Group I to the Fifth Assessment Report of the Intergovernmental Panel on Climate Change*, pages 659–740. [Stocker, T.F., D. Qin, G.-K. Plattner, M. Tignor, S.K. Allen, J. Boschung,

A. Nauels, Y. Xia, V. Bex and P.M. Midgley (eds.)] Cambridge University Press, Cambridge, United Kingdom and New York, NY, USA.

Parmentier, F.-J. W. and Christensen, T. R. (2013). Arctic: speed of methane release. *Nature*, 500(7464):529.

Parmentier, F.-J. W., Christensen, T. R., Sørensen, L. L., Rysgaard, S., Mcguire, A. D., Miller, P. A., and Walker, D. A. (2013). The impact of lower sea-ice extent on Arctic greenhouse-gas exchange. *Nature Climate Change*, 3(3):195–202.

Petrescu, A. M. R., Lohila, A., Tuovinen, J.-P., Baldocchi, D. D., Desai, A. R., Roulet, N. T., Vesala, T., Dolman, A. J., Oechel, W. C., Marcolla, B., Friborg, T., Rinne, J., Matthes, J. H., Merbold, L., Meijide, A., Kiely, G., Sottocornola, M., Sachs, T., Zona, D., Varlagin, A., Lai, D. Y. F., Veenendaal, E., Parmentier, F.-J. W., Skiba, U., Lund, M., Hensen, A., van Huissteden, J., Flanagan, L. B., Shurpali, N. J., Grünwald, T., Humphreys, E. R., Jackowicz-Korczyński, M., Aurela, M. A., Laurila, T., Grüning, C., Corradi, C. A. R., Schrier-Uijl, A. P., Christensen, T. R., Tamstorf, M. P., Mastepanov, M., Martikainen, P. J., Verma, S. B., Bernhofer, C., and Cescatti, A. (2015). The uncertain climate footprint of wetlands under human pressure. *Proceedings of the National Academy of Sciences*, 112(15):4594–4599.

Pirk, N., Mastepanov, M., Parmentier, F.-J. W., Lund, M., Crill, P., and Christensen, T. R. (2015a). Calculations of automatic chamber flux measurements of methane and carbon dioxide using short time series of concentrations. *Biogeosciences Discussions*, 12(17):14593–14617.

Pirk, N., Santos, T., Gustafson, C., Johansson, A. J., Tufvesson, F., Parmentier, F.-j. W., Mastepanov, M., and Christensen, T. R. (2015b). Methane emission bursts from permafrost environments during autumn freeze-in : New insights from ground-penetrating radar. *Geophysical Research Letters*, 42(16):6732–6738.

R Core Team (2015). *RStudio: Integrated Development Environment for R*. RStudio, Inc., Boston, MA.

Rogerson, P. R. (2001). *Statistical methods for geography*. SAGE Publications, London.

Saito, K., Zhang, T., Yang, D., Marchenko, S., Barry, R. G., Romanovsky, V., and Hinzman, L. (2013). Influence of the physical terrestrial Arctic in the eco-climate system. *Ecological Applications*, 23(8):1778–1797.

Schuur, E. a. G., Abbott, B. W., Bowden, W. B., Brovkin, V., Camill, P., Canadell, J. G., Chanton, J. P., Chapin, F. S., Christensen, T. R., Ciais, P., Crosby, B. T., Czimczik, C. I., Grosse, G., Harden, J., Hayes, D. J., Hugelius, G., Jastrow, J. D., Jones, J. B., Kleinen, T., Koven, C. D., Krinner, G., Kuhry, P., Lawrence, D. M., McGuire, a. D., Natali, S. M., O'Donnell, J. a., Ping, C. L., Riley, W. J., Rinke, a., Romanovsky, V. E., Sannel, a. B. K., Schädel, C., Schaefer, K., Sky, J., Subin, Z. M., Tarnocai, C., Turetsky, M. R., Waldrop, M. P., Walter Anthony, K. M., Wickland, K. P., Wilson, C. J., and Zimov, S. a. (2013). Expert assessment of vulnerability of permafrost carbon to climate change. *Climatic Change*, 119(2):359–374.

Schuur, E. A. G., Bockheim, J., Canadell, J. P., Euskirchen, E., Field, C. B., Goryachkin, S. V., Kuhry, P., Lafleur, P. M., Lee, H., Mazhitova, G., Nelson, F. E., Rinke, A., Romanovsky, V. E., Shiklomanov, N., Tarnokai, C., Venevsky, S., Vogel, J. G., and Zimov, S. A. (2008). Vulnerability of permafrost carbon to climate change: Implications for the global carbon cycle. *BioScience*, 58(8):701–714.

Schuur, E. a. G., McGuire, a. D., Schädel, C., Grosse, G., Harden, J. W., Hayes, D. J., Hugelius, G., Koven, C. D., Kuhry, P., Lawrence, D. M., Natali, S. M., Olefeldt, D., Romanovsky, V. E., Schaefer, K., Turetsky, M. R., Treat, C. C., and Vonk, J. E. (2015). Climate change and the permafrost carbon feedback. *Nature*, 520(7546):171–179.

Serreze, M. C. and Francis, J. A. (2006). The arctic amplification debate. *Climate Change*, 76(3):241–264.

Shakhova, N., Semiletov, I., Leifer, I., Sergienko, V., Salyuk, A., Kosmach, D., Chernykh, D., Stubbs, C., Nicolsky, D., Tumskoy, V., and Gustafsson, Ö. (2013). Ebullition and storm-induced methane release from the East Siberian Arctic Shelf. *Nature Geoscience*, 7(January):64–70.

Stocker, T., D. Qin, G.-K., Plattner, L., Alexander, S., Allen, N., Bindoff, F.-M., Bréon, J., Church, U., Cubasch, S., Emori, P., Forster, P., Friedlingstein, N., Gillett, J., Gregory, D., Hartmann, E., Jansen, B., Kirtman, R., Knutti, K., Krishna Kumar, P., Lemke, J., Marotzke, V., Masson-Delmotte, G., Meehl, I., Mokhov, S., Piao, V., Ramaswamy, D., Randall, M., Rhein, M., Rojas, C., Sabine, D., Shindell, L., Talley, D., Xie, V., and S.-P. (2013). Technical Summary. In *Climate Change 2013: The Physical Science Basis. Contribution of Working Group I to the Fifth Assessment Report of the Intergovernmental Panel on Climate Change*, pages 33–115. [Stocker, T.F., D. Qin, G.-K. Plattner, M. Tignor, S.K. Allen, J. Boschung, A. Nauels, Y. Xia, V. Bex and P.M. Midgley (eds.)] Cambridge University Press, Cambridge, United Kingdom and New York, NY, USA.

Ström, L., Falk, J. M., Skov, K., Jackowicz-Korczynski, M., Mastepanov, M., Christensen, T. R., Lund, M., and Schmidt, N. M. (2015). Controls of spatial and temporal variability in CH4 flux in a high arctic fen over three years. *Biogeochemistry*, 125(1):21–35.

Ström, L., Tagesson, T., Mastepanov, M., and Christensen, T. R. (2012). Presence of Eriophorum scheuchzeri enhances substrate availability and methane emission in an Arctic wetland. *Soil Biology and Biochemistry*, 45:61–70.

Tagesson, T., Mastepanov, M., Mölder, M., Tamstorf, M. P., Eklundh, L., Smith, B., Sigsgaard, C., Lund, M., Ekberg, A., Falk, J. M., Friborg, T., Christensen, T. R., and Ström, L. (2013). Modelling of growing season methane fluxes in a high-Arctic wet tundra ecosystem 1997 2010 using in situ and high-resolution satellite data. *Tellus*, 65(19722):1–21.

Tagesson, T., Mölder, M., Mastepanov, M., Sigsgaard, C., Tamstorf, M. P., Lund, M., Falk, J. M., Lindroth, A., Christensen, T. R., and Ström, L. (2012). Land-atmosphere exchange of methane from soil thawing to soil freezing in a high-Arctic wet tundra ecosystem. *Global Change Biology*, 18(6):1928–1940.

Tamstorf, M. P., Iversen, K. M., Hansen, B. U., Sigsgaard, C., Kaufmann, L. R. H., Holm, N., Andreasen, R. H., Mastepanov, M., Strøm, L., and Christensen, T. R. (2008). Nuuk Basic: The GeoBasic Programme. In *Nuuk Ecological Research Operations 1 st Annual Report , 2007*, chapter 3, pages 1–112. [Jensen, L. M. and Rasch, M. (eds.)], Copenhagen, Danish Polar Centre, Danish Agency for Science, Technology and Innovation, Ministry of Science, Technology and Innovation.

Tang, J., Miller, P. a., Persson, a., Olefeldt, D., Pilesjö, P., Heliasz, M., Jackowicz-Korczynski, M., Yang, Z., Smith, B., Callaghan, T. V., and Christensen, T. R. (2015). Carbon budget estimation of a subarctic catchment using a dynamic ecosystem model at high spatial resolution. *Biogeosciences*, 12(9):2791–2808.

Thorsøe, K., Tamstorf, M. P., Aastrup, P., Mikkelsen, D. M., and Rasch, M. (2008). Executive Summary. In *Nuuk Ecological Research Operations 1 st Annual Report , 2007*, chapter 0. [Jensen, L. M. and Rasch, M. (eds.)], Copenhagen, Danish Polar Centre, Danish Agency for Science, Technology and Innovation, Ministry of Science, Technology and Innovation.

Vaughan, D., Comiso, J., Allison, I., Carrasco, J., Kaser, G., Kwok, R., Mote, P., Murray, T., Paul, F., Ren, J., Rignot, E., Solomina, O., Steffen, K., and Zhang, T. (2013). Observations: Cryosphere. In *Climate Change 2013: The Physical Science Basis. Contribution of Working Group I to the Fifth Assessment Report of the Intergovernmental Panel on Climate Change*, pages 317–382. [Stocker, T.F., D. Qin, G.-K. Plattner, M. Tignor, S.K. Allen, J. Boschung, A. Nauels, Y. Xia, V. Bex and P.M. Midgley (eds.)] Cambridge University Press, Cambridge, United Kingdom and New York, NY, USA.

Appendix A Additional figures

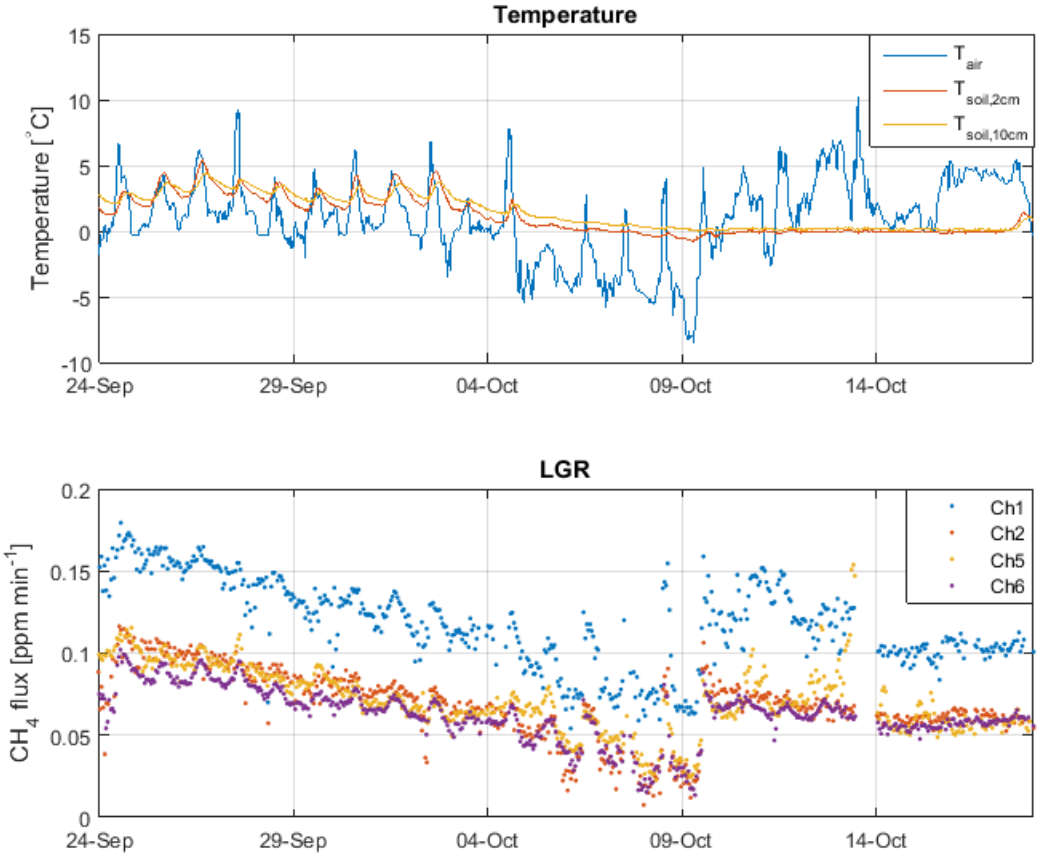

Figure A15: Air and soil temperature, at 2 and 10 cm depth, as well as the CH_4 fluxes from the LGR for the time period 24th of September to 18th of October. Observe how the fluxes increase as the temperatures go up after the 9th of October.

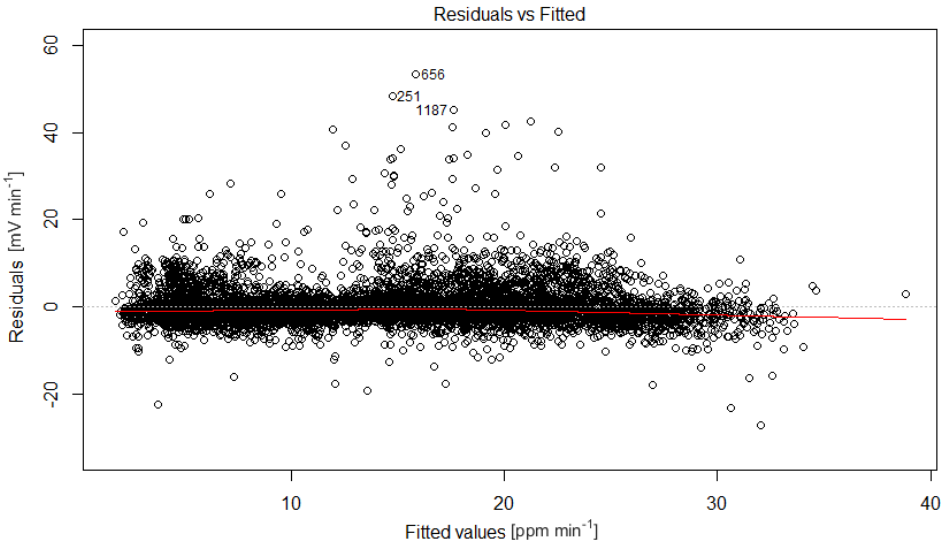

Figure A16: The residual from the fitted line from the regression of the ΔRH-filtered data. The outliers are clearly visible, but the general spread in the residuals is relatively constant.

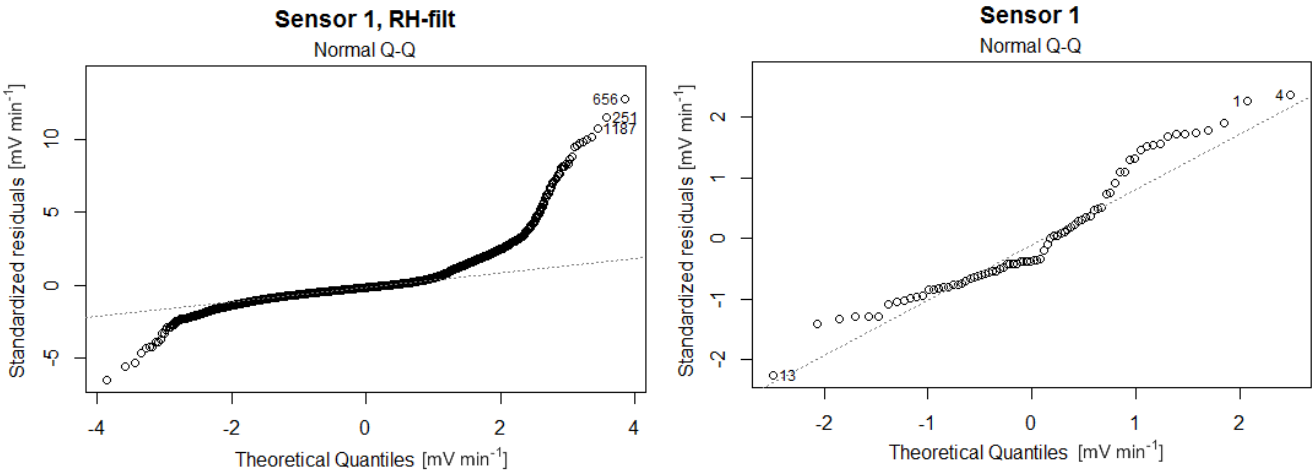

(a) ΔRH-filtered data **(b)** ΔRH-filtered daily data

Figure A17: Quantile-quantile plots for first order polynomial regressions of respective dataset. More curvature is seen in the large dataset (**a**) than in the daily data (**b**). This indicates that the daily data is closer to a normal distribution.

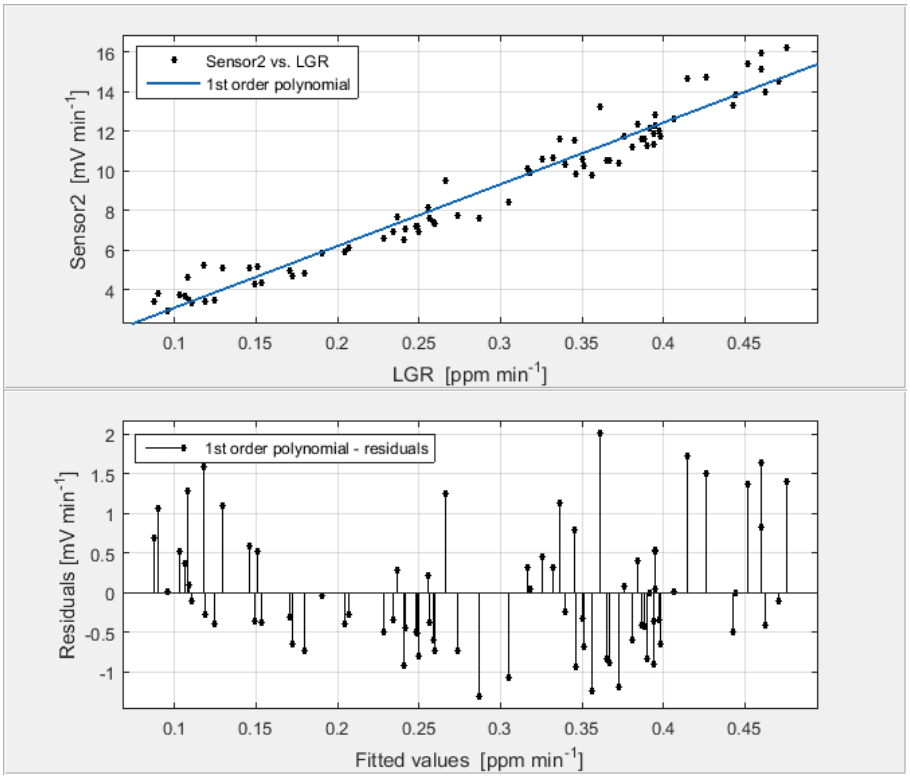

Figure A18: 1st order polynomial regression of the daily data, Sensor 2. y = 31.11x -0.015, R^2=0.96.

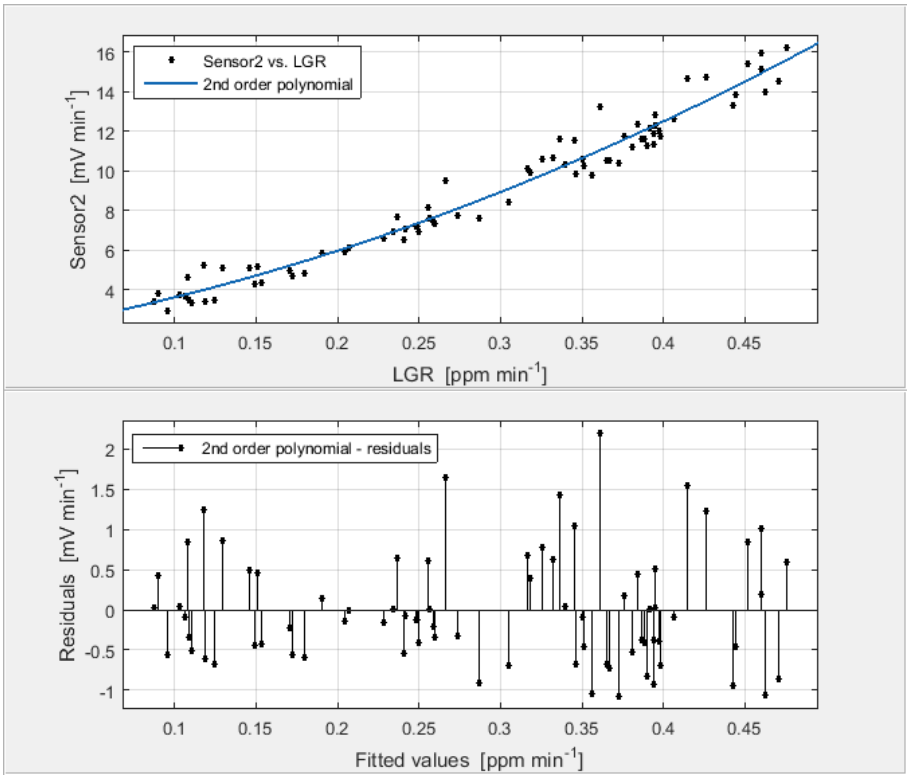

Figure A19: 2nd order polynomial regression of the daily data, Sensor 2. y = 30.25x^2 + 14.45x + 1.87 with R^2=0.96.

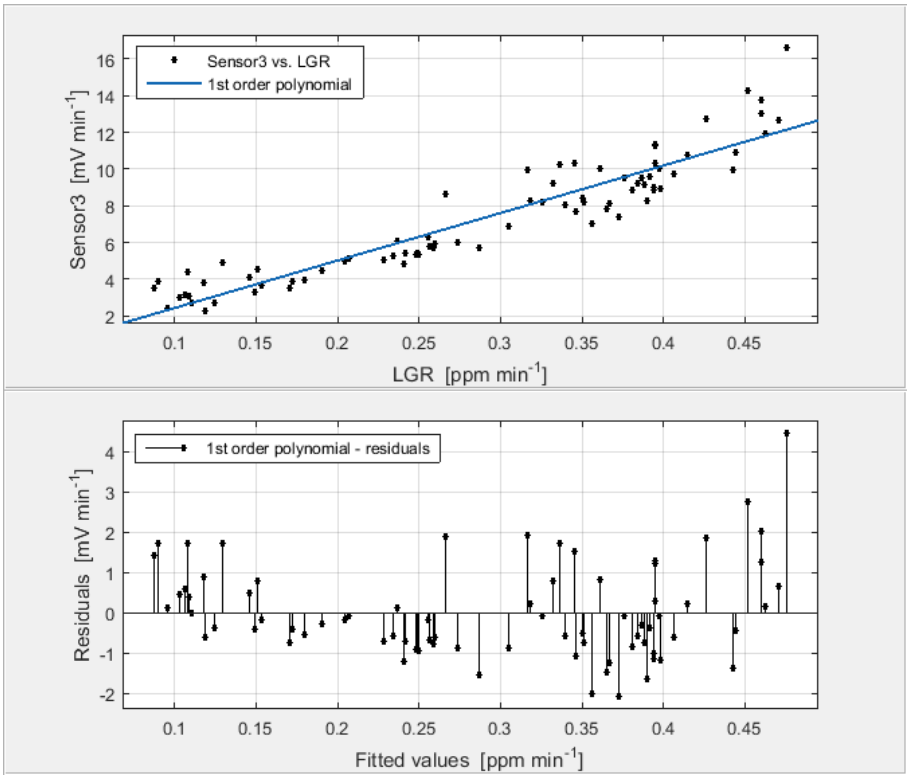

Figure A20: 1st order polynomial regression of the daily data, Sensor 3. y = 25.87x-0.153, R^2=0.87.

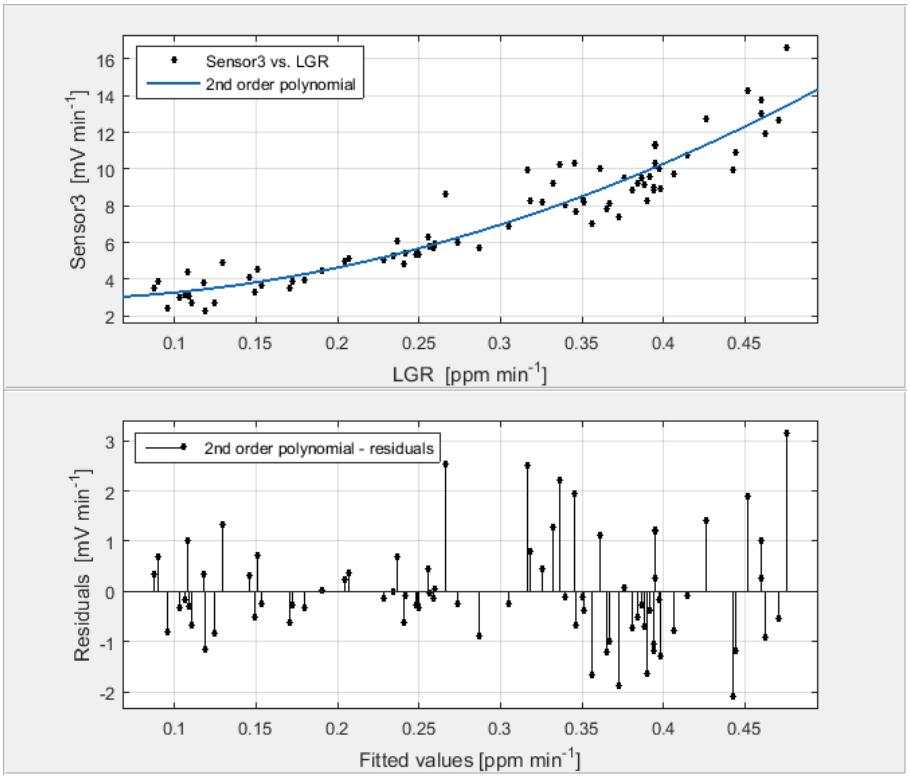

Figure A21: 2nd order polynomial regression of the daily data, Sensor 3. y = 48.99 x^2 + -1.11x + 2.90 with R^2=0.90.

Institutionen för naturgeografi och ekosystemvetenskap, Lunds Universitet.

Student examensarbete (Seminarieuppsatser). Uppsatserna finns tillgängliga på institutionens geobibliotek, Sölvegatan 12, 223 62 LUND. Serien startade 1985. Hela listan och själva uppsatserna är även tillgängliga på LUP student papers (https://lup.lub.lu.se/student-papers/search/) och via Geobiblioteket (www.geobib.lu.se)

The student thesis reports are available at the Geo-Library, Department of Physical Geography and Ecosystem Science, University of Lund, Sölvegatan 12, S-223 62 Lund, Sweden. Report series started 1985. The complete list and electronic versions are also electronic available at the LUP student papers (https://lup.lub.lu.se/student-papers/search/) and through the Geo-library (www.geobib.lu.se)

350 Mihaela – Mariana Tudoran (2015) Occurrences of insect outbreaks in Sweden in relation to climatic parameters since 1850

351 Maria Gatzouras (2015) Assessment of trampling impact in Icelandic natural areas in experimental plots with focus on image analysis of digital photographs

352 Gustav Wallner (2015) Estimating and evaluating GPP in the Sahel using MSG/SEVIRI and MODIS satellite data

353 Luisa Teixeira (2015) Exploring the relationships between biodiversity and benthic habitat in the Primeiras and Segundas Protected Area, Mozambique

354 Iris Behrens & Linn Gardell (2015) Water quality in Apac-, Mbale- & Lira district, Uganda - A field study evaluating problems and suitable solutions

355 Viktoria Björklund (2015) Water quality in rivers affected by urbanization: A Case Study in Minas Gerais, Brazil

356 Tara Mellquist (2015) Hållbar dagvattenhantering i Stockholms stad - En riskhanteringsanalys med avseende på långsiktig hållbarhet av Stockholms stads dagvattenhantering i urban miljö

357 Jenny Hansson (2015) Trafikrelaterade luftföroreningar vid förskolor – En studie om kvävedioxidhalter vid förskolor i Malmö

358 Laura Reinelt (2015) Modelling vegetation dynamics and carbon fluxes in a high Arctic mire

359 Emelie Linnéa Graham (2015) Atmospheric reactivity of cyclic ethers of relevance to biofuel combustion

360 Filippo Gualla (2015) Sun position and PV panels: a model to determine the best orientation

361 Joakim Lindberg (2015) Locating potential flood areas in an urban environment using remote sensing and GIS, case study Lund, Sweden

362 Georgios-Konstantinos Lagkas (2015) Analysis of NDVI variation and snowmelt around Zackenberg station, Greenland with comparison of ground data and remote sensing.

363 Carlos Arellano (2015) Production and Biodegradability of Dissolved Organic Carbon from Different Litter Sources

364 Sofia Valentin (2015) Do-It-Yourself Helium Balloon Aerial Photography - Developing a method in an agroforestry plantation, Lao PDR

365 Shirin Danehpash (2015) Evaluation of Standards and Techniques for Retrieval of Geospatial Raster Data - A study for the ICOS Carbon Portal

366 Linnea Jonsson (2015) Evaluation of pixel based and object based classification

methods for land cover mapping with high spatial resolution satellite imagery, in the Amazonas, Brazil.

367 Johan Westin (2015) Quantification of a continuous-cover forest in Sweden using remote sensing techniques

368 Dahlia Mudzaffar Ali (2015) Quantifying Terrain Factor Using GIS Applications for Real Estate Property Valuation

369 Ulrika Belsing (2015) The survival of moth larvae feeding on different plant species in northern Fennoscandia

370 Isabella Grönfeldt (2015) Snow and sea ice temperature profiles from satellite data and ice mass balance buoys

371 Karolina D. Pantazatou (2015) Issues of Geographic Context Variable Calculation Methods applied at different Geographic Levels in Spatial Historical Demographic Research -A case study over four parishes in Southern Sweden

372 Andreas Dahlbom (2016) The impact of permafrost degradation on methane fluxes - a field study in Abisko

373 Hanna Modin (2016) Higher temperatures increase nutrient availability in the High Arctic, causing elevated competitive pressure and a decline in *Papaver radicatum*

374 Elsa Lindevall (2016) Assessment of the relationship between the Photochemical Reflectance Index and Light Use Efficiency: A study of its seasonal and diurnal variation in a sub-arctic birch forest, Abisko, Sweden

375 Henrik Hagelin and Matthieu Cluzel (2016) Applying FARSITE and Prometheus on the Västmanland Fire, Sweden (2014): Fire Growth Simulation as a Measure Against Forest Fire Spread – A Model Suitability Study –

376 Pontus Cederholm (2016) Californian Drought: The Processes and Factors Controlling the 2011-2016 Drought and Winter Precipitation in California

377 Johannes Loer (2016) Modelling nitrogen balance in two Southern Swedish spruce plantations

378 Hanna Angel (2016) Water and carbon footprints of mining and producing Cu, Mg and Zn: A comparative study of primary and secondary sources

379 Gusten Brodin (2016) Organic farming's role in adaptation to and mitigation of climate change - an overview of ecological resilience and a model case study

380 Veränika Trollblad (2016) Odling av *Cucumis Sativus* L. med aska från träd som näringstillägg i ett urinbaserat hydroponiskt system

381 Susanne De Bourg (2016) Tillväxteffekter för andra generationens granskog efter tidigare genomförd kalkning

382 Katarina Crafoord (2016) Placering av energiskog i Sverige - en GIS analys

383 Simon Nåfält (2016) Assessing avalanche risk by terrain analysis An experimental GIS-approach to The Avalanche Terrain Exposure Scale (ATES)

384 Vide Hellgren (2016) Asteroid Mining - A Review of Methods and Aspects

385 Tina Truedsson (2016) How does the amount of snow and wind conditions effect water pressure measurements during winter in a lake in western Greenland?

386 Chloe Näslund (2016) Prompt Pediatric Care Pediatric patients' estimated travel times to surgically-equipped hospitals in Sweden's Scania County

387 Yufei Wei (2016) Developing a web-based system to visualize vegetation trends by a nonlinear regression algorithm

388 Greta Wistrand (2016) Investigating the potential of object-based image analysis to identify tree avenues in high resolution aerial imagery and lidar data

389 Jessica Ahlgren (2016) Development of a Web Mapping Application for grazing resource information in Kordofan, Sudan, by downloading MODIS data automatically via Python

390 Hanna Axén (2016) Methane flux measurements with low-cost solid state sensors in Kobbefjord, West Greenland